

Using ALS data for biomass estimations alongside forest roads

A case study in Uppsala Municipality

Raul Fernandez Lacruz and Liviu Theodor Ene



Inventory of overgrown vegetation on a forest roadside in Björklinge (Uppsala). Photographer: Michael Krook.

Preface	3
Summary	4
Sammanfattning.....	5
Background and aim of the study.....	6
Materials and methods	8
Study area and airborne laser scanning (ALS) data	8
Road network data	9
Fieldwork data collection.....	10
Auxiliary data at field subplot level	13
Canopy height model (CHM) segmentation	13
Analyses of fieldwork data.....	14
Predictive statistical models	15
Results.....	17
Regression models	17
Prediction of forest inventory attributes	18
Harvesting potential	22
Discussion and conclusions.....	23
Methodology	23
Biomass potential and economic profitability	24
References	26
Appendix	30
Appendix 1. Summary of forest inventory data of subplots (transects).	30
Appendix 2. STAN model formulation.	34



Uppsala Science Park, 751 83 Uppsala
 skogforsk@skogforsk.se
 skogforsk.se

Kvalitetsgranskning (Intern peer review) har genomförts 27 oktober 2022 av
 Maria Iwarsson Wide, programchef. Därefter har Magnus Thor, Forskningschef,
 granskat och godkänt publikationen för publicering den 28 november 2022.

Redaktör: Leslie Walke, leslie@communicaid.se
 ©Skogforsk 2022 ISSN 1404-305X

Preface

This study has been carried out during the period 2021–2022 within the work package “National potentials of biomass from low-value trees” as a part of the project “Potentials, values and costs for society and companies when felling low-value trees”. The project was financed by the Swedish Energy Agency (project number 45923-1).

We gratefully acknowledge our colleagues Michael Krook and Jens Lindberg at Skogforsk for data collection during fieldwork.

Sävar 2022–06–17

Raul Fernandez Lacruz

Uppsala 2022–06–17

Liviu Theodor Ene

Summary

Low-value trees can be defined as trees growing on a site where they have a potential or actual negative impact on the site's other values. Felling of low-value trees can be justified, to benefit either infrastructure or natural values. Examples of such trees are found along infrastructure features such as power line corridors, roadsides, and edges of railway lines.

Airborne laser scanning (ALS) data opens new possibilities for application at different levels of forest planning, and ALS could be used to estimate nationwide potentials of low-value trees. The aim of our study was to predict tree diameter at breast height, tree height, and biomass of low-value trees along forest roadsides in a case study in Uppsala Municipality. Free-of-charge, publicly available ALS data from the Swedish Mapping, Cadastral and Land Registration Authority (Lantmäteriet) was combined with road network data for Functional Road Classes (FRC) 7, 8 and 9 (i.e., forest roads). A clearing buffer, extending 5 m on each side of the delineated trafficable road zone, was defined. A forest inventory with 10-m² transects on a sample of 100 forest roadsides was conducted. ALS and inventory data was analysed to build prediction models of diameter, height, and biomass.

The methodology demonstrated that forest vegetation attributes along the forest road network can be estimated with reasonable accuracy when field and temporally consistent ALS data is available. From a management point of view, the models with ALS data could be useful for visualising the general state of vegetation on relatively large areas, and assist in the planning of road maintenance activities. However, the methodology does not provide a solution for long-term monitoring, as the ALS data used in this study is updated every 8–10 years. If the ALS data is not updated, the model predictions cannot be used to monitor the vegetation development in areas of interest. Other sources of remotely sensed data should be considered in addition to ALS, e.g., digital imagery data provided by the national aerial surveys performed by Lantmäteriet, raster height products, and orthomosaics, so that vegetation maps can be updated more frequently (for instance, every 2–4 years).

Results showed that 55% of biomass volume was found along roadsides of FRC 9, 40% in road class 8, and 5% in road class 7. Based on model predictions, the biomass density averaged 24 dry tonnes per km of forest road in the case study area, totalling 630 km of forest roads. The estimated annual harvest potential according to the expected clearing frequencies of each road class amounted to 12 GWh per year, assuming a clearing width of 5 m on each roadside. The annual harvest potential was upscaled to the entire Uppsala County (containing 13,284 km of forest roads), and was 356 GWh per year if the same biomass density as in the case study area was assumed. If a narrower clearing width of 2 m was considered, the annual harvest potential decreased to 142 GWh per year.

The relatively small tree sizes and low biomass density would incur high harvesting costs due to the low cutting productivity, which combined with current prices for forest chips would not allow a profitable harvest. Conventional practices (such as chain/flail mowers mounted on tractors) without biomass recovery are likely to prevail for the management of low-value trees along roadsides, unless there is a substantial increase in wood chip prices and advances in harvesting technologies.

Sammanfattning

Lågvärdesträd är träd som, på grund av sin växtplats, har en faktisk eller potentiellt negativ effekt på platsens andra värden. Avverkning av lågvärdesträd kan motiveras för att gynna antingen infrastruktur eller naturvård. Det kan handla om träd som växer längs infrastrukturobjekt så som kraftledningsgator, vägkanter och järnvägskanter.

Data från luftburen laserskanning (på engelska, *airborne laser scanning, ALS*) öppnar nya möjligheter som kan tillämpas på olika nivåer av skoglig planering, och exempelvis användas för att uppskatta rikstäckande potentialer av lågvärdesträd. Syftet med vår studie var att förutsäga trädiameter på brösthöjd, trädhöjd och därigenom biomassa från lågvärdesträd längs skogsbivägar i en fallstudie i Uppsala kommun. Kostnadsfria, offentligt ALS-data från Lantmäteriet kombinerades med vägnätsdata för funktionella vägklasser 7, 8 och 9 (dvs. skogsbivägar). En röjningsbuffert som sträckte sig 5 m på vardera sida av vägen definierades. En skogsinventering med 10 m²-transekter på ett urval av 100 vägkanter genomfördes. ALS- och inventeringsdata analyserades för att skapa prediktionsmodeller för diameter, höjd och biomassa.

Metoden visade att prediktionen av skogliga parametrar längs skogsbivägar är möjlig med rimlig noggrannhet när både fält- och ALS-data är tidskonsistenta (dvs. data representerar ungefär samma tidsperiod). Ur skötselperspektiv kan de presenterade modellerna vara användbara för att visualisera vegetationens allmänna tillstånd på relativt stora områden och hjälpa till vid planeringen av vägunderhållsåtgärder. Metoden ger dock ingen lösning för långtidsuppföljning, eftersom ALS-data som vi använde i studien uppdateras med 8–10 års mellanrum. Om ALS-data inte uppdateras oftare är det inte möjligt att använda prognoserna för att övervaka vegetationsutvecklingen i fallstudieområdet eller andra områden. Andra källor till fjärranalysdata bör övervägas utöver ALS. Till exempel digitala flygbildsdata från Lantmäteriets nationella flygundersökningar, rasterhöjdsprodukter och ortomosaik, så att vegetationskartor kan uppdateras med kortare mellanrum (2–4 år).

I analysen konstaterades att 55 procent av volymen biomassa återfanns längs kanterna till vägar med funktionell klass 9, 40 procent för klass 8 och 5 procent för klass 7. Baserat på modellprognoser beräknades en genomsnittlig biomassadensitet på 24 ton torrsubstans per km väg inom fallstudieområdet, som innehar 630 km skogsbivägar. Med hänsyn till de förväntade röjningsfrekvenserna för varje vägklass och en röjningsbredd på 5 m på vardera sida av vägen, skulle en biomassapotential på 12 GWh per år kunna skördas inom fallstudieområdet. Avverkningspotentialen beräknades för hela Uppsala län (som innehar 13 284 km skogsbivägar) och motsvarade 356 GWh per år, om man antar samma biomassadensitet som i fallstudieområdet. Skulle en smalare röjningsbredd på 2 m appliceras så skulle potentialen minska till 142 GWh per år.

De relativt klena träd och den låga biomassadensitet skulle dock ge höga avverkningskostnader på grund av den låga produktiviteten vid avverkning, som i kombination med rådande priser på skogsflis, inte skulle möjliggöra en lönsam skörd. Det kan således förväntas att konventionell praxis (oftast kättingslagor monterade på traktorer) utan biomassauttag, kommer att dominera skötseln av lågvärdesträd längs skogsbivägar, om det inte sker en rejäl ökning av flispriserna och framsteg inom avverkningstekniken.

Background and aim of the study

Low-value trees can be defined as trees growing on a site where they have a potential or actual negative impact on the site's other values. Felling of low-value trees can be justified, to benefit either infrastructure or natural values. Examples of such trees are found along infrastructure features such as power line corridors, roadsides, and edges of railway lines (Figure 1). This vegetation often consists of small-diameter trees, currently without almost any industrial use (as they are normally below pulpwood dimensions), but with a potential use for bioenergy and biorefinery applications (Emanuelsson et al. 2014). For traffic safety reasons and to maintain the functionality of the infrastructure, these trees are normally cleared on a regular basis, using chain/flail mowers mounted on tractors or wheel loaders, or with brush saws (Forsberg 2010). However, high harvesting costs together with low prices paid for this biomass prevents larger industrial utilisation, and biomass is normally left to rot *in situ* (Fernandez Lacruz 2019).



Figure 1. Forest roadsides after clearance in northern Sweden.

Available geodata (Willén 2021), such as airborne laser scanning (ALS) data (Anon 2022b), has revolutionised forest inventories (Lindgren et al. 2021) and opened new possibilities for application at different levels of forest planning. The national ALS data survey is carried out by the Swedish Mapping, Cadastral and Land Registration Authority (Lantmäteriet), with an updating frequency of about 7 years and covering about 75% of the Swedish land area (approximately 350,000 km²). Earlier studies (Iwarsson Wide 2013) have used ALS data to develop a method to support planning of biofuel harvest in neglected young forest in edge zones along roads and young forest stands. ALS data could therefore assist in the quantification of nationwide potentials of low-value trees. The estimation of forest attributes such as diameter at breast height (DBH) and tree height could help in the planning of vegetation management and road maintenance operations.

The aim of our study was to predict DBH, height and biomass of low-value trees along forest roadsides using ALS data in a case study in Uppsala Municipality.

Materials and methods

Study area and airborne laser scanning (ALS) data

The study area covered ~47,000 hectares (ha), located in the north-western part of Uppsala Municipality (Figure 2). This area was chosen due to the availability of ALS data from the most recent survey (2018–2021) and a workforce to perform an on-ground forest inventory.

The ongoing acquisition campaign of ALS data provided a point density of approximately 1–2 points per m², with up to five returns per pulse classified as ground, water, low or high point, or unclassified (Anon 2022b). In forested areas, it is assumed that the unclassified returns are the vegetation hits. The ALS data was downloaded from Lantmäteriet as compressed .LAZ files, and the 3D point clouds were processed to obtain (1) canopy height models (CHM) at 0.5 m resolution, and (2) a set of features that can be used as auxiliary information for building predictive models for the inventory attributes. The geoprocessing of ALS point clouds was performed using the R-package “lidR” (Roussel et al. 2020, Roussel & Auty 2021) of the R statistical software (R Core Team 2021). The spatial distribution of the ALS survey regions carried out during 2018–2021 for the study area is shown in Figure 2. ALS data was acquired using a Leica ALS80-HP8236 airborne scanner.

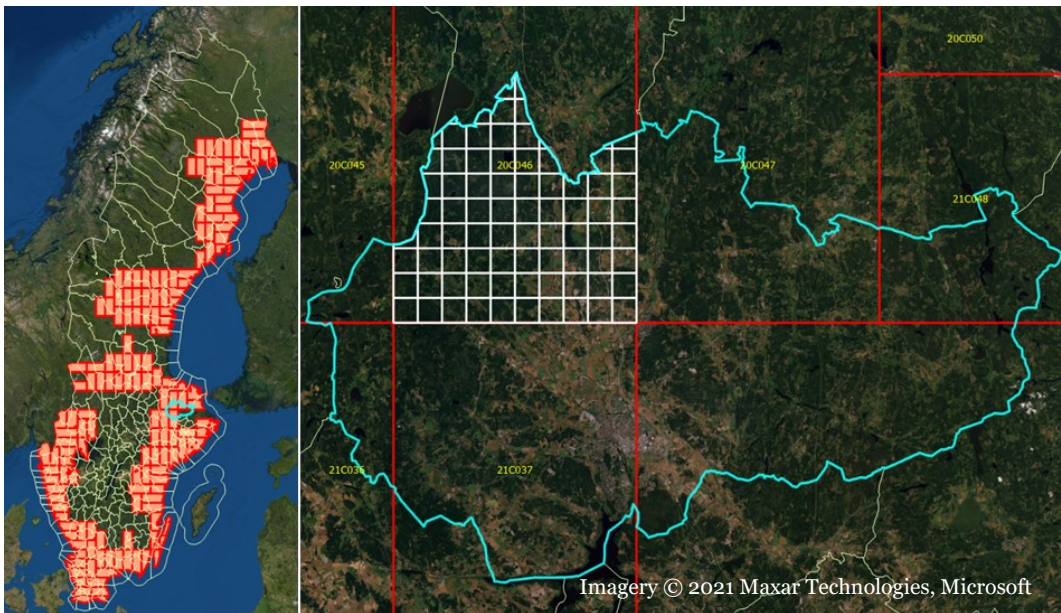


Figure 2. The coverage of the country-wide ALS scanning for 2018–2021. The left image shows the scanned areas (red polygons), overlaying the Swedish administrative regions, with Uppsala Municipality outlined in pale blue. The right image provides a more detailed overview of the selected study region in Uppsala Municipality, with the white polygons representing the 2.5 × 2.5 km tiles used for the granular storage of ALS data, and the annually scanned areas (red polygons) labelled in yellow. “20C046” refers to the case study area.

Road network data

The Swedish road network consists of approximately 140,000 km of public roads and 430,000 km of private roads (Skogskunskap 2021a). About half of the private roads (210,000 km) are classified as forest roads, and are used primarily by the forestry industry for transporting wood raw material and by other stakeholders for hunting, recreation, etc. Depending on their use and maintenance, the roads registered in the National Road Database (NVDB) are classified into nine functional road classes (FRC), where classes 7, 8 and 9 refer to forest roads (Skogskunskap 2021b; Davidsson 2020). NVDB is a service managed by the Swedish Transport Administration (Trafikverket) and additional information is provided for the forest road network (SNVDB) (Biometria, 2022).

- **Class 7** (main road – *huvudväg*): these roads represent the backbone of the forest road network, directly connected to the main state (public) road network. These roads are scheduled for annual maintenance.
- **Class 8** (normal road – *normalväg*): these roads are an intermediary layer connecting the roads in classes 7 and 9. These roads are scheduled for regular maintenance (for example, every 4 years).
- **Class 9** (null road - *nollväg*): these roads are the innermost ones, in the outer branches of the road network or as isolated short links. These roads normally lack a plan for regular maintenance, meaning that they are only maintained when the road needs to be used by traffic, e.g., when forest measures are planned.

The spatial distribution of the forest road network in the study area is shown in Figure 3 and summarised in Table 1. The shapefiles containing the forest road network were obtained from the NVDB.

Table 1. Summary statistics for the road transects by Functional Road Class.

Aggregation	Statistics	Functional Road Class				Total
		Main roads	Normal roads	Null roads		
		7	8	9		
	Total	110	661	1,668	2,439	
Road transects	mean	0.29	0.38	0.21	0.26	
	Length (km)	SD ⁽¹⁾	0.29	0.42	0.26	0.32
	Total	31.84	251.85	345.97	629.66	
	mean	0.4	0.49	0.29	0.35	
	Area (ha)	SD ⁽¹⁾	0.52	0.71	0.44	0.54
	Total	43.54	324.9	483.96	852.41	

⁽¹⁾ Standard deviation

The trafficable road zone was defined as a 4 m-buffer along the central road line. The decision to use a 4-m width was supported by exploratory results obtained after performing measurements in orthophoto aerial mosaics on different road segments in FRC 7-9 in the study area. The vegetated area investigated was then restricted to a buffer (henceforth called vegetation buffer) extending 5 m on each side of the delineated trafficable road zone.

The Swedish Transport Administration recommends a vegetation-free zone with a minimum distance of 2 m horizontally and 4.6 m vertically from the roadbed (Trafikverket 2019). Other guidelines also suggest a vegetation-free zone of 2–3 m on

each side of the road (Skogskunskap 2016). Earlier potential estimations and machine studies of biomass harvest have reported buffers extending between 2.5–7.5 m on each roadside (Emanuelsson et al. 2014; Fernandez-Lacruz et al. 2020; Iwarsson Wide 2009a, 2009b, 2013). The chosen 5-m vegetation buffer attempted to reflect the practice when the aim is to harvest biomass instead of just clearing and leaving the biomass on the ground.

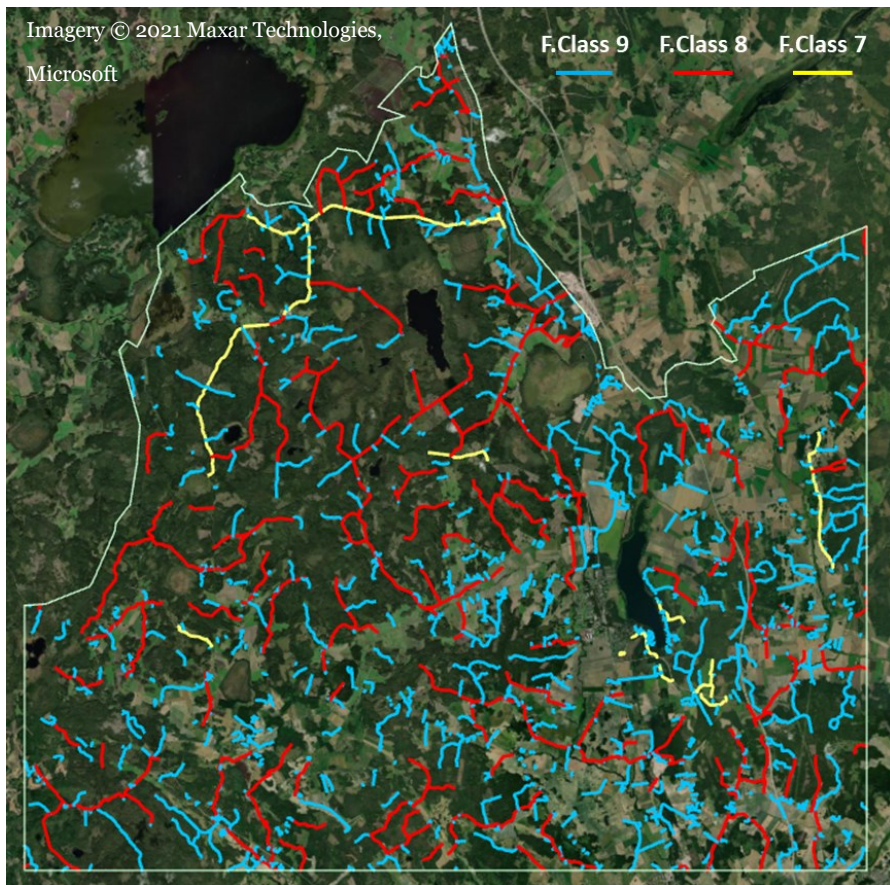


Figure 3. The forest road network (FRC 7, 8 and 9) across the study area (white border).

Fieldwork data collection

A forest inventory was performed between 11–15 October 2021 in the study area (Figure 3) by a crew of two field technicians. The inventory consisted of 100 transects, 2×5 m (10 m^2), hereafter referred to as subplots. The subplots were placed in pairs, one on each side of the road selected for sampling, and perpendicular to the road's direction. The subplot started at the point where the roadway ended (i.e., where vegetation started to grow) and extended 5 m towards the adjacent forest (i.e., encompassing the previously defined vegetation buffer). The coordinates (x, y, z) of each subplot were registered with GPS at the start and end points (Figure 4) to determine the exact direction and slope of the subplots. In each subplot, the DBH, height and species of trees that had reached breast height (≥ 1.3 m) and with a DBH ≥ 1 cm, were recorded. The subplots were also divided into five 1-m sections (denoted A-B-C-D-E) and the position of every tree was registered. Tree height was measured for three trees per subplot.

To expedite the field work, the country-wide 2.5×2.5 km ALS data tiling system was used to geographically restrict the locations of the field samples (i.e., the subplots along the roads). The sample size was set to 10 tiles, so that the crew could cover two tiles a day, corresponding to 10 plots (or 20 subplots) per tile, thereby amounting to 100 subplots. The tiles were selected using the R-package “BalancedSampling” (Grafström & Liscic 2019), with the median ALS echo height extracted from the vegetation buffers within each tile as the auxiliary variable. The selected tiles are shown in Figure 5, and an example of georeferenced field plots with two 2×5 m subplots configuration is shown in Figure 6.

The forest inventory aimed to document the variation in biomass density in the study area, by surveying roadsides with “low” and “high” density. For this reason, instead of deciding the placement of the subplots beforehand, the field technicians were given the task to explore the forest roads within the ten selected sample tiles (Figure 5) and decide where to place the subplots, according to the observed variation.

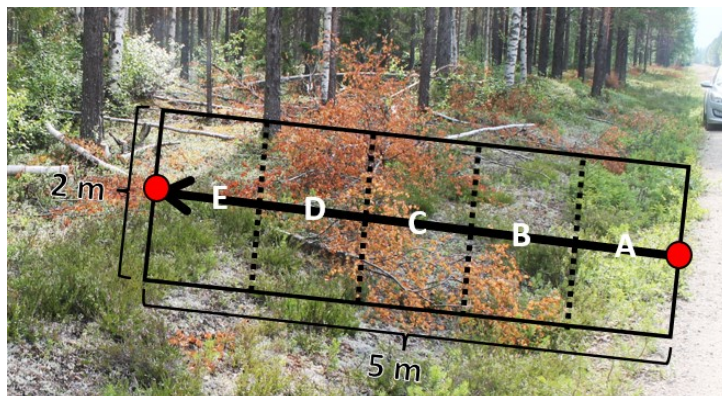


Figure 4. Sketch of a subplot. The red dots indicate the points where GPS coordinates were registered, and A-B-C-D-E denotes the sections of the subplot.

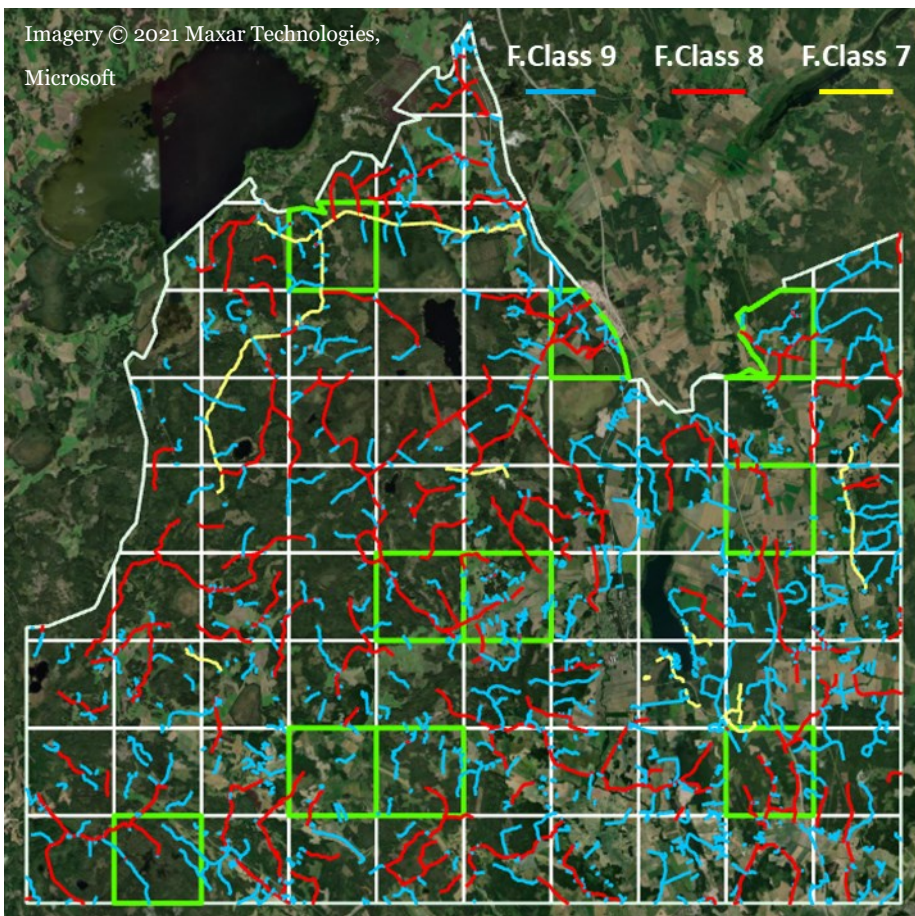


Figure 5. The 2.5×2.5 km ALS tile partitioning system overlain (white polygons) over the network of forest roads (FRC 7, 8 and 9). The tiles for field data acquisition are highlighted in light green.

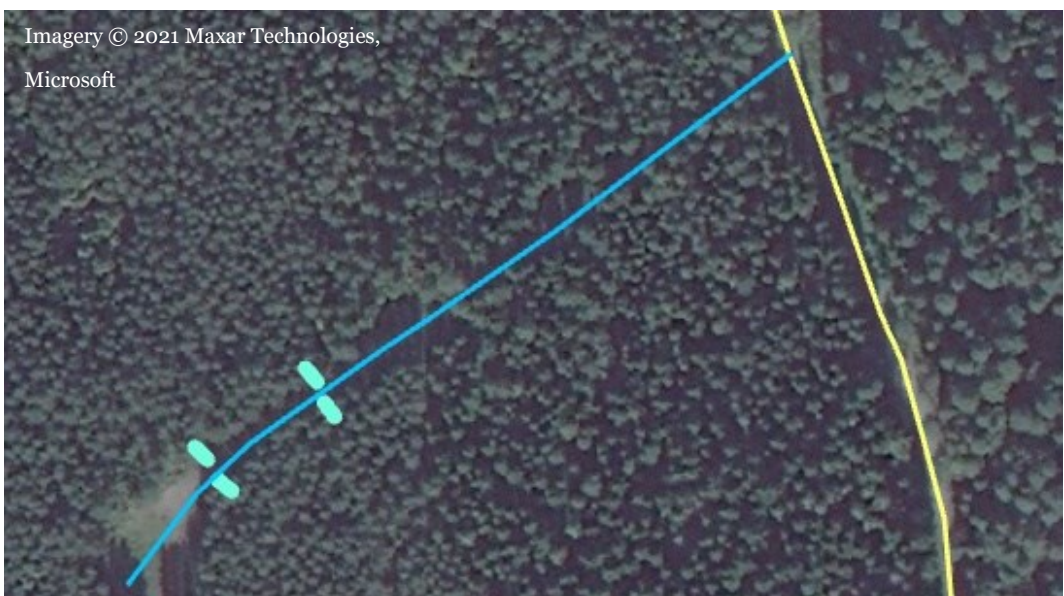


Figure 6. Placement of the field plots (highlighted in light blue) with two subplots configuration along a road segment in FRC 9.

Auxiliary data at field subplot level

On each subplot, several descriptors for the vertical distribution of the vegetation were extracted from the height distributions of the 3D ALS point clouds: the percentiles corresponding to the 0.75 and 0.95 quantiles, the standard deviations, and the proportion of points above one-third of the maximum echo height.

Canopy height model (CHM) segmentation

To extract similar ALS auxiliaries on the areas not included in the field sample, the 0.5-m resolution CHM within the vegetation buffer was delineated into contiguous, non-overlapping segments using image segmentation techniques. The CHM segmentation was performed using the Adaptive Simple Linear Iterative Clustering (SLICO) algorithm (Achanta et al. 2012) applied to the 8-bit normalised (0-255) CHM. SLICO is an image segmentation algorithm that groups the raster cells into sets (superpixels) that are homogeneous in terms of size and compactness and correspond relatively well with the local content such as boundaries and object contours (Achanta et al. 2012, Li et al. 2021). Images with complex structures can be thereby efficiently represented using a smaller number of primitives, as each superpixel is supposed to encapsulate meaningful content. The delineation was performed using the SLICO implementation offered by the R-package “OpenImageR” (Mouselimis 2021).

The segmentation was performed independently for each road transect. The road transects were represented as undirected, acyclic graphs, with the superpixels as the nodes and the adjacency relationships represented by the edges, followed by spatial clustering of the nodes using the walktrap community finding algorithm (Pons & Latapy 2005) implemented in the “igraph” R-package (Csardi & Nepusz 2006). An output of the delineation algorithm is shown in Figure 7, and a summary in Table 2.

Table 2. Summary of segmentation results, by Functional Road Class.

Aggregation	Statistics	Functional Road Class			
		Main roads	Normal roads	Null roads	Total
CHM segments	Total	43,816	328,030	489,554	861,400
	min	1.75	1.75	1.5	1.50
	max	28	31.75	33.5	33.50
	mean	9.94	9.9	9.89	9.90
	SD ⁽¹⁾	2.23	2.35	2.28	2.30

⁽¹⁾ Standard deviation

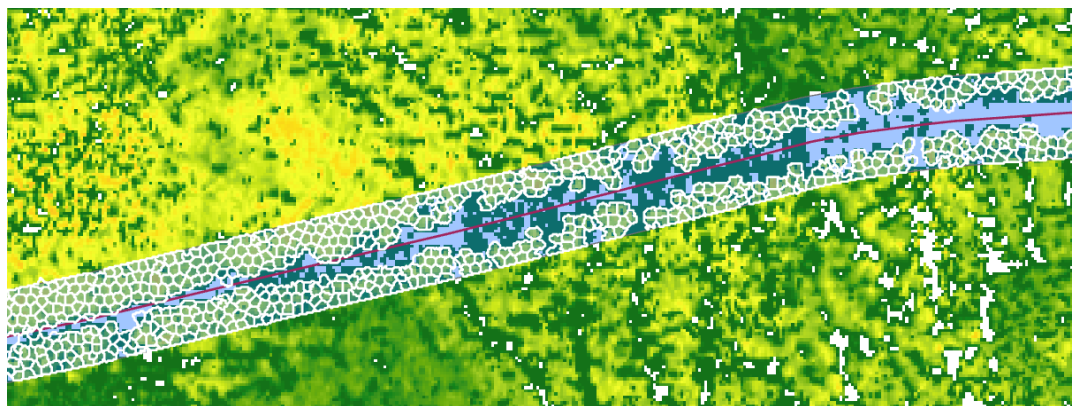


Figure 7. Canopy height models (CHM) delineated into segments using the SLICO algorithm. The segment boundaries (in white) are overlain on the vegetation buffer (light blue).

Analyses of fieldwork data

Height-diameter models were derived for tree species with nonlinear mixed effects models, using the R-package “nlme” (Pinheiro et al. 2022). The total above-ground biomass for every tree, dry tonnes (t), was calculated with the biomass functions from Marklund (1988), denoted AGB_M , and Repola & Ulvcrona (2014), denoted AGB_U . Birch biomass functions were used for all broadleaves. Mean values for inventory attributes (to be used in subsequent predictive models with ALS data) were calculated for each subplot and are shown in Appendix 1. A summary of these attributes is also shown in Table 3. Table 4 summarises the distribution of tree species, showing a dominance of broadleaves. The DBH of the majority (85%) of measured trees during fieldwork was below 4 cm (Figure 8). Analysis of biomass distribution amongst the defined sections of the subplots showed that ~40% of the biomass volume was found within a buffer of 2 m from the roadway, and more than 80% within a buffer of 4 m (Figure 9).

Table 3. Summary of forest inventory attributes (all subplots, n=100).

	DBH ⁽¹⁾ (cm)		Height (m)		Stand density (trees ha ⁻¹)	Biomass density (dry t ha ⁻¹)	
	Arithmetic	Basal-area weighted	Arithmetic	Basal-area weighted		Marklund (AGB_M)	Repolo & Ulvcrona (AGB_U)
Min	1.2	1.3	2.2	2.1	1,000	0.7	0.6
Max	6.2	9.8	7.0	9.3	52,000	132.9	121.5
Mean	2.6	4.0	3.7	4.6	10,606	21.5	18.8
SD ⁽²⁾	1.0	2.1	0.9	1.6	7,638	24.5	21.3

⁽¹⁾ DBH = diameter at breast height, i.e. at 1.3 m above ground level.

⁽²⁾ SD= standard deviation

Table 4. Summary of tree species composition (% of number of measured trees).

Species	%
Aspen (<i>Populus tremula</i>)	8.7
Birch (<i>Betula spp.</i>)	30.1
Black alder (<i>Alnus glutinosa</i>)	5.5
Norway spruce (<i>Picea abies</i>)	9.8
Rowan (<i>Sorbus aucuparia</i>)	7.2
Scots pine (<i>Pinus sylvestris</i>)	1.9
Willow (<i>Salix spp.</i>)	27.6
Other ⁽¹⁾	9.2

⁽¹⁾ Most other species comprised ash (*Fraxinus excelsior*), juniper (*Juniperus communis*), European oak (*Quercus robur*), maple (*Acer platanoides*) and fir (*Abies spp.*).

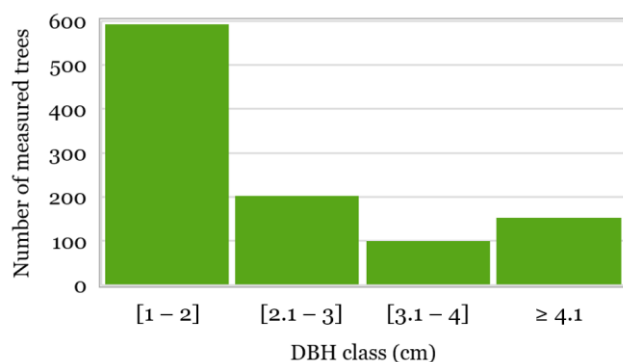


Figure 8. Average distribution of diameter at breast height (DBH) classes (cm) in the subplots (all measured trees, i.e., those that had reached heights of 1.3 m).

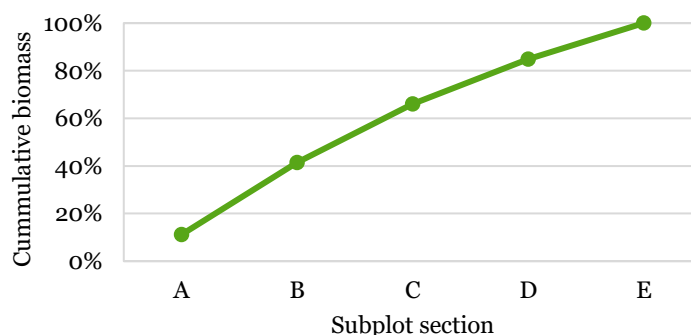


Figure 9. Cumulative percentage of total biomass in the defined 1-m sections in the subplots.

Predictive statistical models

The parametric models for predicting the target inventory attributes, arithmetic average tree height (H), arithmetic average diameter at breast height (DBH), and above-ground biomass (AGB_M and AGB_U), were formulated as mixed generalised additive models (GAMM), assuming a Gaussian distribution of the responses and log-link functions. The random effects were formulated as varying plot-level intercepts correlated among models.

The covariates used for constructing the basis-functions in each model are shown in Table 5. Low-rank isotropic thin plate regression splines (Wood 2003) were used as smooth functions for the model covariates.

Since all the models were built from the same dataset and contained some common covariates, it was natural to assume that they also shared a common residual covariance structure. In such situations, an efficient approach estimating the model parameters is the seemingly unrelated regression (SUR) (Zellner 1962, Zellner & Ando 2010). With SUR, the set of regression equations is solved simultaneously as a system of equations. Given the complex covariance structures assumed for the models, the SUR estimation was performed in a Bayesian framework using the Hamiltonian Markov Chain Monte Carlo inference engine provided by the R-package “*brms*” (Bürkner 2017, 2018, 2021), which offers a convenient wrapping to the STAN probabilistic programming language (Carpenter et al. 2017). The STAN formulation of the fitted models is provided in Appendix 2.

Results

Regression models

The summary of the Bayesian R-squared estimates for the regression models (Gelman et al. 2018) produced using the “brms” R-package is shown in Table 5. The quantile-quantile plots for empirical versus fitted values using the group-level effects (unconditional) and population-level (conditional, i.e., using only the fixed part of the model’s) predictions, are shown in Figure 10 and Figure 11.

Table 5. Bayesian R-squared summaries for the fitted regression models.

Attribute	Bayesian R-squared estimates			
	Estimate	Estimated error	2.5 Q	97.5 Q
Unconditional predictions				
H	0.53	0.06	0.40	0.63
DBH	0.68	0.05	0.56	0.76
AGB _U	0.89	0.01	0.86	0.91
AGB _M	0.88	0.01	0.85	0.90
Conditional predictions				
H	0.35	0.05	0.24	0.45
DBH	0.41	0.05	0.30	0.49
AGB _U	0.37	0.06	0.25	0.47
AGB _M	0.37	0.05	0.26	0.47

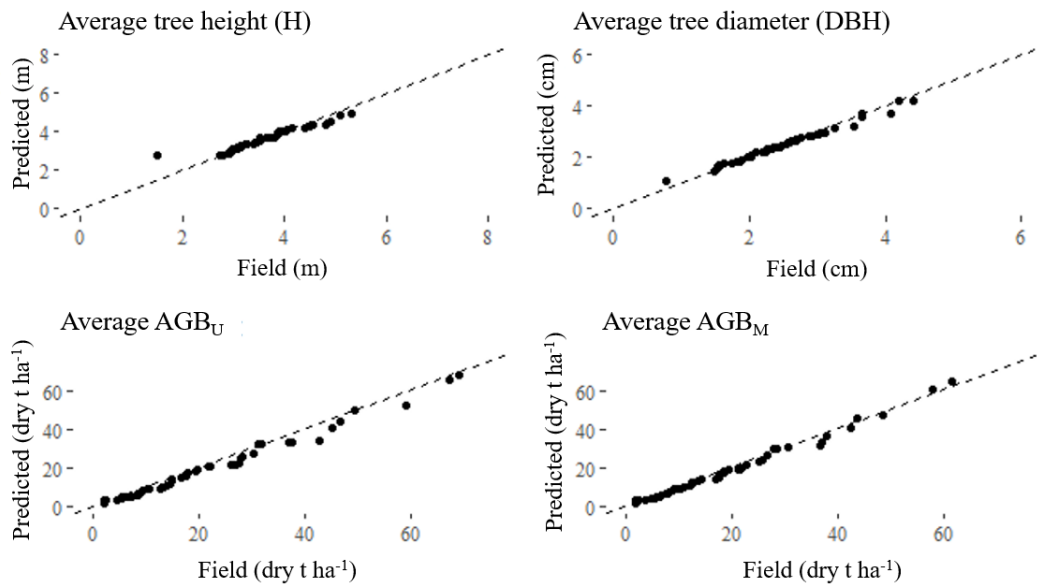


Figure 10. Q-Q plots for empirical and model predictions for the plot-level inventory attributes including the random effects (unconditional).

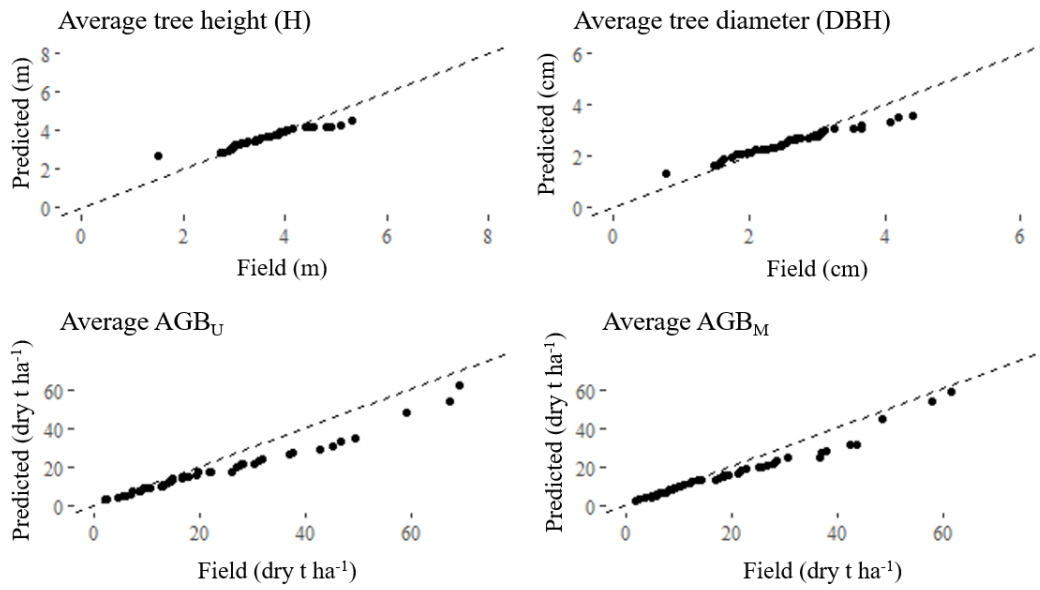


Figure 11. Q-Q plots for empirical and model marginal predictions for the plot-level inventory attributes.

Prediction of forest inventory attributes

Point estimates of the forest inventory attributes (H , DBH, AGB_M , AGB_U) and their uncertainty were produced at segment level (Table 6), and aggregated estimates were compiled by road transects (Table 7) and FRC 7, 8 and 9 (Table 8-10, respectively), using 1,000 random draws from the posterior distributions of the fitted models. The point estimates were calculated as the average of the sampling distributions, and the uncertainties were expressed as their inter-quartile ranges and standard deviation (SD).

Table 6. Summary of predicted attributes and their uncertainties at segment level. The percentages were calculated relative to the predicted average values.

Segment-level attributes	Summary statistics				
	mean	SD	min	max	range
Area (ha)	9.93	2.26	4.25	33.5	29.25
Expected values of the posterior predictive distribution					
H (m)	3.66	0.58	1.46	5.54	4.07
DBH (cm)	2.58	0.89	0.83	5.99	5.16
AGB_M (dry t ha ⁻¹)	23.7	14.05	0.96	76.87	75.91
AGB_U (dry t ha ⁻¹)	22.14	13.56	0.78	76.15	75.37
Standard deviations					
H (m)	0.29	0.07	0.14	1.2	1.05
H (%)	8.05	2.03	4.27	37.83	33.56
DBH (cm)	0.42	0.16	0.18	1.31	1.14
DBH (%)	11.52	3.6	4.63	55.06	50.43
AGB_M (dry t ha ⁻¹)	6.86	6.61	1.03	41.28	40.24
AGB_M (%)	31.83	14.56	16.42	233.48	217.06
AGB_U (dry t ha ⁻¹)	6.38	6.23	0.91	37.12	36.21

	(%)	31.61	14.43	16.37	197.68	181.31
Interquartile range						
H	(m)	0.39	0.1	0.18	1.83	1.65
	(%)	10.74	2.73	5.36	49.2	43.84
DBH	(cm)	0.55	0.22	0.23	2.45	2.22
	(%)	23.56	9.41	8.99	58.57	49.58
AGB _M	(dry t ha ⁻¹)	8.94	9.23	0.85	73.82	72.97
	(%)	40.88	18.06	20.48	102.49	82.01
AGB _U	(dry t ha ⁻¹)	8.33	8.91	0.78	67.89	67.11
	(%)	40.48	17.87	20.63	101.18	80.54

⁽¹⁾Standard deviation

Table 7. Summary of predicted attributes and their uncertainties at road transect level. The percentages were calculated relative to the predicted average values.

Transect-level attributes	Summary statistics					
	mean	SD	min	max	range	
Area (ha)	0.35	0.54	0	6.32	6.32	
Expected values of the posterior predictive distribution						
H	(m)	3.71	0.16	2.36	4.27	1.9
DBH	(cm)	2.66	0.33	0.95	4.6	3.66
AGB _M	(dry t ha ⁻¹)	24.79	4.46	2.99	46.5	43.52
AGB _U	(dry t ha ⁻¹)	23.29	4.27	2.65	45.15	42.5
Standard deviations						
H	(m)	0.18	0.02	0.12	0.42	0.3
	(%)	4.8	0.64	3.26	12.47	9.2
DBH	(cm)	0.28	0.06	0.15	0.71	0.55
	(%)	10.56	2.41	6.08	31.52	25.44
AGB _M	(dry t ha ⁻¹)	5.25	1.61	1.55	21.06	19.51
	(%)	21.18	4.69	16.24	59.04	42.8
AGB _U	(dry t ha ⁻¹)	4.94	1.59	1.48	19.7	18.22
	(%)	21.17	4.66	15.95	60.93	44.98
Interquartile ranges						
H	(m)	0.24	0.03	0.16	0.54	0.38
	(%)	6.42	0.87	4.42	17.33	12.91
DBH	(cm)	0.37	0.08	0.21	1.04	0.83
	(%)	13.99	3.15	7.99	41.6	33.62
AGB _M	(dry t ha ⁻¹)	6.95	2.06	2.03	25.9	23.87
	(%)	28.09	5.92	20.44	73.86	53.42
AGB _U	(dry t ha ⁻¹)	6.45	1.99	1.81	26.17	24.36
	(%)	27.69	5.76	20.37	77.19	56.82

⁽¹⁾Standard deviation

Table 8. Summary of predicted attributes and their uncertainties for the road transects in FRC 7. The percentages were calculated relative to the predicted average values.

Transect-level attributes	Summary statistics				
	mean	SD	min	max	range
Area (ha)	0.4	0.52	0	3.94	3.93
Expected Values of the Posterior Predictive Distribution					
H (m)	3.66	0.18	3.01	4.24	1.24
DBH (cm)	2.56	0.37	1.56	4.61	3.05
AGB _M (dry t ha ⁻¹)	23.21	5.28	6.44	46.1	39.67
AGB _U (dry t ha ⁻¹)	21.76	5.05	6.31	46.15	39.84
Mean absolute deviations					
H (m)	0.18	0.03	0.12	0.42	0.31
(%)	4.77	0.75	3.39	10.57	7.18
DBH (cm)	0.26	0.06	0.17	0.66	0.48
(%)	10.12	2	6.17	14.63	8.47
AGB _M (dry t ha ⁻¹)	4.9	1.92	1.57	20.55	18.98
(%)	21.1	4.55	16.63	44.57	27.93
AGB _U (dry t ha ⁻¹)	4.57	1.91	1.43	20.48	19.06
(%)	20.93	4.42	16.37	44.38	28.01
Interquartile range					
H (m)	0.23	0.04	0.16	0.56	0.4
(%)	6.38	1.02	4.52	13.95	9.43
DBH (cm)	0.34	0.09	0.23	1.02	0.79
(%)	13.46	2.71	7.97	22.13	14.16
AGB _M (dry t ha ⁻¹)	6.56	2.48	2.18	26.48	24.3
(%)	28.26	5.61	22.36	57.43	35.07
AGB _U (dry t ha ⁻¹)	6.06	2.52	1.89	26.41	24.52
(%)	27.73	5.8	21.38	57.22	35.84

⁽¹⁾ Standard deviation

Table 9. Summary of predicted attributes and their uncertainties for the road transects in FRC 8. The percentages were calculated relative to the predicted average values.

Transect-level attributes	Summary statistics				
	mean	SD	min	max	range
Area (ha)	0.49	0.71	0	6.32	6.32
Expected Values of the Posterior Predictive Distribution					
H	(m)	3.71	0.15	2.84	4.15
DBH	(cm)	2.64	0.32	1.5	4.32
AGB _M	(dry t ha ⁻¹)	24.77	4.41	6.49	42.35
AGB _U	(dry t ha ⁻¹)	23.18	4.19	6.51	41.93
Mean absolute deviations					
H	(m)	0.18	0.02	0.13	0.29
	(%)	4.81	0.55	3.52	7.86
DBH	(cm)	0.27	0.06	0.16	0.6
	(%)	10.46	2.38	6.39	23.37
AGB _M	(dry t ha ⁻¹)	5.1	1.54	1.64	18.74
	(%)	20.59	4.32	16.27	51.21
AGB _U	(dry t ha ⁻¹)	4.77	1.5	1.51	18.09
	(%)	20.53	4.18	16.32	50.23
Interquartile range					
H	(m)	0.24	0.03	0.16	0.4
	(%)	6.42	0.75	4.54	10.57
DBH	(cm)	0.36	0.08	0.21	0.94
	(%)	13.84	3.11	8.36	31.16
AGB _M	(dry t ha ⁻¹)	6.78	2.01	2.12	25.37
	(%)	27.42	5.46	20.97	64.14
AGB _U	(dry t ha ⁻¹)	6.27	1.96	2.01	25.53
	(%)	26.99	5.34	21	64.92

⁽¹⁾ Standard deviation

Table 10. Summary of predicted attributes and their uncertainties for the road transects in FRC 9. The percentages were calculated relative to the predicted average values.

Transect-level attributes	Summary statistics				
	mean	SD	min	max	range
Area (ha)	0.29	0.44	0	5.69	5.68
Expected Values of the Posterior Predictive Distribution					
H (m)	3.71	0.16	2.36	4.28	1.92
DBH (cm)	2.67	0.34	0.97	4.12	3.16
AGB _M (dry t ha ⁻¹)	24.91	4.42	2.91	38.43	35.52
AGB _U (dry t ha ⁻¹)	23.44	4.24	2.62	38.64	36.02
Mean absolute deviations					
H (m)	0.18	0.02	0.12	0.36	0.24
(%)	4.81	0.67	3.42	12.55	9.13
DBH (cm)	0.28	0.06	0.16	0.75	0.59
(%)	10.61	2.44	6.16	31.24	25.08
AGB _M (dry t ha ⁻¹)	5.33	1.62	1.59	18.95	17.36
(%)	21.42	4.85	15.85	61.43	45.58
AGB _U (dry t ha ⁻¹)	5.03	1.6	1.45	18.41	16.97
(%)	21.41	4.81	16.23	62.79	46.56
Interquartile range					
H (m)	0.24	0.03	0.15	0.48	0.33
(%)	6.43	0.92	4.36	17.65	13.29
DBH (cm)	0.37	0.08	0.22	0.99	0.77
(%)	14.08	3.22	8.06	42.37	34.31
AGB _M (dry t ha ⁻¹)	7.06	2.06	2.07	21.46	19.39
(%)	28.39	6.11	20.71	75.01	54.3
AGB _U (dry t ha ⁻¹)	6.57	1.98	1.91	19.81	17.9
(%)	28	5.92	20.76	75.84	55.08

(1) Standard deviation

Harvesting potential

Based on model predictions, the total biomass volume for the entire case study area (containing 630 km of forest roads) was 15,120 dry t. Five percent of the biomass volume was found in roadsides along FRC 7, 40% in road class 8, and 55% in road class 9. On average, the biomass density was 24 dry t per km of forest road. If we assume that biomass from FRC 7 must be harvested every year, class 8 every 5 years, and class 9 every 15 years, the estimated annual harvesting potential would be ~12 GWh per year, assuming a clearing width of 5 m on each roadside, a moisture content of 50%, and a conversion factor of 4.7 MWh dry t⁻¹ (Nylander & Kockum, 2016). The harvesting potential was upscaled to the entire Uppsala County (containing 13,284 km of forest roads), producing a figure of ~356 GWh per year if the same biomass density as in the case study area was assumed. If a narrower clearing width of 2 m was considered, the annual potential decreased to ~142 GWh per year.

Discussion and conclusions

Methodology

The applied methodology demonstrated that forest vegetation attributes along the forest road network can be estimated with reasonable accuracy when field and temporally consistent ALS data is available. Table 7 showed an average uncertainty in the estimation of forest attributes of 5% for tree height, 11% for DBH, and 21% for biomass. These values of uncertainty can be considered relatively small and manageable, given the scale and the purpose of the models. The resulting maps provide a snapshot, geotagged information on the vegetation state (Figure 12). From a management point of view, the models with ALS data could be useful for visualising the general state of vegetation on relatively large areas and assist in the strategic planning of road maintenance activities. A similar approach could be applied to determine the need for pre-commercial thinning in forest stands and to locate areas to prioritise.

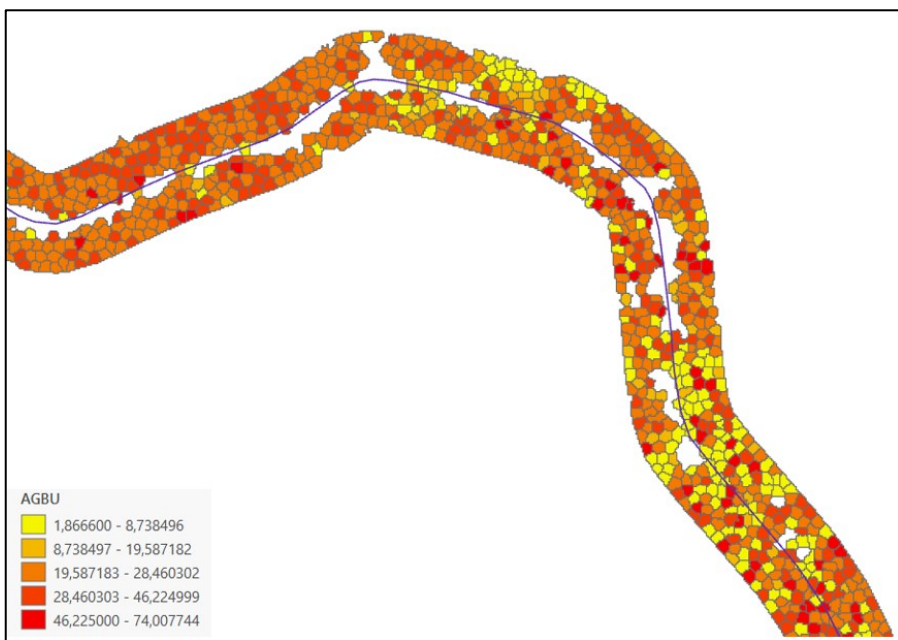


Figure 12. Heatmap of modelled biomass density ($AGBU$, dry $t\ ha^{-1}$) on the roadsides of a forest road in the study area. Predictions of tree DBH and height can also be represented in similar heatmaps.

However, the methodology does not provide a solution for long-time monitoring, as it cannot provide updates on the changes affecting the vegetation, i.e. the vegetation growth and clearing activities. The periodicity of vegetation clearing activities along roads varies across geographical regions, ownership categories, and FRC. This implies that the vegetation changes with different temporal frequencies, and these changes need to be incorporated in the vegetation maps. While the vegetation states due to clearings could be easily updated, the monitoring of vegetation growth is not possible without temporally consistent remote sensing data.

The ALS data required for building the predictive models is updated every 8–10 years. If the ALS data is not updated, the model predictions cannot be used for monitoring the

vegetation development in the areas of interest. Other sources of remotely sensed data should therefore be considered in addition to ALS. For instance, digital imagery data provided by the national aerial surveys performed by Lantmäteriet (Anon 2022c) and raster height products and ortho-mosaics (Anon 2022d) could be used between consecutive ALS surveys, which would enable vegetation maps to be updated more frequently (2–4 years).

This study did not consider the time since the last clearing of the surveyed forest roadsides, meaning that some roadsides were recently cleared while others were cleared some years ago. This could explain part of the variation in the vegetation state (Appendix 1). However, the variation can also be due to the site fertility and conditions of the adjacent forest stands, as the inventory subplots extended in a buffer area of 5 m from the road edge, partly inside the neighbouring forests in some cases. The models should include indicators that can be regarded as crucial for making decisions on whether or not to clear a forest road. Examples of these indicators can be the position of the branches in relation to the road, assuring that minimum horizontal (2 m) and vertical (4.6 m) vegetation-free distances in relation to the roadbed (Trafikverket 2019) are fulfilled.

Biomass potential and economic profitability

The models showed that 5% of the biomass volumes in the case study area were found along roads in FRC 7, 40% in roads of class 8, and 55% in class 9. This distribution of biomass could be expected, as roadsides in class 9 roads are only meant to be cleared when the road needs to be used by traffic after forest operations such as thinning or final felling (Skogskunskap 2021a). As Figure 9 showed, the potential increased steadily across the width of the clearing buffer, meaning that it would decrease accordingly if narrower buffers were set. However, the calculated annual harvesting potential would depend on the clearing frequency of each road, and would vary according to the FRC and responsibility of road management.

The average surveyed DBH, height, and biomass density (Table 3, Appendix 1) were in line with earlier surveys of low-value trees in power line corridors and forest roadsides in Sweden (Fernandez-Lacruz et al. 2013, 2020; Iwarsson Wide 2009a, 2009b). Cost-revenue models presented in previous studies (which used a harvester equipped with an accumulating felling head and a forwarder to extract the biomass) showed that a mechanised harvest of small trees in power line corridors and roadsides can become cost-competitive where mean tree heights are at least 6–7 m. Consequently, this means that at least 80% of the surveyed forest roadsides in our study would lack economic profitability (Appendix 1), given current forest fuel prices. Therefore, it can be expected that conventional clearing practices without biomass recovery (such as chain/flail mowers attached to tractors) will prevail for vegetation management along forest roads, unless there is a substantial increase in wood chip prices and advances in the development of harvesting technologies. One way to increase the cost-efficiency of harvest of small-diameter trees could be the development of technology for continuous cutting and accumulation, as shown by Iwarsson Wide et al. (2021).

Calculations of profitability of biomass harvest along forest roadsides, considering the whole supply chain, were carried out with the web-based tool “Profitability of harvesting small trees and bushes” (*Lönsamhet vid avverkning av sly*) (Grönlund 2021). In the example, based on a density of 10,000 trees per ha, an average DBH of 4 cm, a small range in tree size, a road segment of 250 m, an energy price of SEK 195 per MWh (average price for forest chips at heating plats in 2021, Energimyndigheten 2022), and default settings, the calculation tool returned a loss of SEK 4,963 (Figures 13–15).

Steg 1 - Segment

Ange värden som beskriver den sträcka du står inför att bedöma.

Dela upp sträckan i segment som har liknande egenskaper. Utifrån egenskaperna som du anger visas en bild med dessa egenskaper. Testa olika värden och välj den bild som bäst beskriver ditt segment.

Stamtäthet	10000 (i meter mellan träden)	st/ha
Medeldiameter	Låg (4 cm)	cm
Storleksvariation	Liten	
		
Segmentets längd	250	m
Lägg till		

Figure 13. Step 1, definition of vegetation attributes in the web-based tool “Profitability of harvesting small trees and bushes” (Grönlund 2021).

Steg 2 - Kostnader

Var uppmärksam på vilken enhet som anges. Omräkning mellan olika enheter kan göras med WeCalc. Förs kostnaderna som inte är aktuella, sätt värdet till noll.

Avverkningsmaskinens timkostnad	1200	kr/G ₀ tim
Skördarens förflyttningskostnad	2000	kr per flytt
Skotarens timkostnad	950	kr/G ₀ tim
Skotarens förflyttningskostnad	2000	kr per flytt
Avstånd från avverkningsplats till avlägg	100	m
Sönderdelningskostnad	40	kr/m ³ s
Transportkostnad	40	kr/m ³ s
Energipris	152	kr/m ³ s
Beräkna		

Figure 14. Step 2, definition of supply costs and energy price in the web-based tool “Profitability of harvesting small trees and bushes” (Grönlund 2021).

Förlust: 4963 kr	
Utfall	
Totala intäkter	5257 kr
Totala kostnader	10220 kr
Avverkning	
Avverkad mängd	5.5 ton torrsubstans
Fördelning kostnader	
Avverkningskostnad	4891 kr
Skotningskostnad	2562 kr
Sönderdelningskostnad	1383 kr
Transportkostnad	1383 kr

Figure 15. Step 3, economic results in the web-based tool “Profitability of harvesting small trees and bushes” (Grönlund 2021).

References

- Achanta, R., Shaji, A., Smith, K., Lucchi, A., Fua, P. & Süstrunk, S. 2012. SLIC superpixels compared to state-of-the-art superpixel methods. *IEEE Transactions on Pattern Analysis and Mach Intelligence*, 34, 2274–82.
- Anon. 2022a. Klassning av skogsbilvägar.
https://www.biometria.se/media/fa1ba4qc/klassning-av-skogsbilvaegar_september-2021_webb.pdf.
- Anon. 2022b. Lantmäteriet: Laser data Download, forest.
<https://www.lantmateriet.se/sv/Kartor-och-geografisk-information/geodataprodukter/produktlista/laserdata-nedladdning-skog/#steg=4>.
- Anon. 2022c. Digital aerial photographs.
https://www.lantmateriet.se/globalassets/kartor-och-geografisk-information/flyg--och-satellitbilder/e_pb_dig_flygb.pdf.
- Anon. 2022d. Surface model from aerial photographs.
https://www.lantmateriet.se/globalassets/kartor-och-geografisk-information/hojddata/e_ytmodell_fran_flygbild_v1.3.pdf.
- Biometria. 2022. Skogsbilvägar. Retrieved 2022-06-16 from
<https://www.biometria.se/tjaenster/transport/skogsbilvaegar/>
- Bürkner P. 2017. brms: An R Package for Bayesian Multilevel Models Using Stan. *Journal of Statistical Software*, 80(1), 1–28.
- Bürkner P. 2018. Advanced Bayesian Multilevel Modeling with the R Package brms. *The R Journal*, 10(1), 395–411.
- Bürkner P. 2021. Bayesian Item Response Modeling in R with brms and Stan. *Journal of Statistical Software*, 100, 1–54.

- Carpenter, B., Gelman, A., Hoffman, M.D., Lee, D., Goodrich, B., Betancourt, M., et al. 2017. Stan: A Probabilistic Programming Language. *Journal of Statistical Software* 76(1).
- Csardi, G., Nepusz, T. 2006. The igraph software package for complex network research. *InterJournal, Complex Systems*, 1695. <https://igraph.org>.
- Davidsson, A. 2020. Rätt väginformation avgörande för säkra virkestransporter - Skogforsk, <https://www.skogforsk.se/kunskap/kunskapsbanken/2020/Ratt-vaginformati...>
- Emanuelsson, U., Ebenhard, T., Eriksson, L., Forsberg, M., Hansson, P-A., Hultåker, O., Iwarsson Wide, M., Lind, T., Nilsson, D., Ståhl, G., Andersson, R. 2014. Landsomfattande slytäkt – potential, hinder och möjligheter. Swedish Biodiversity Centre at Swedish University of Agricultural Sciences and Uppsala University.
- Energi myndigheten. 2022. Trädbränsle-, torv- och avfallspriser. <https://www.energi myndigheten.se/statistik/den-officiella-statistiken/statistikprodukter/tradbransle--och-torvpriser/>
- Fernandez-Lacruz, R., Di Fulvio, F., & Bergström, D. 2013. Productivity and profitability of harvesting power line corridors for bioenergy. *Silva Fenn*, 47(1), id 904.
- Fernandez Lacruz, R. 2019. Improving supply chains for logging residues and small-diameter trees in Sweden. *Acta Universitatis Agriculturae Sueciae* 2019, doctoral thesis number 2019:44. Department of Forest Biomaterials and Technology, Swedish University of Agricultural Sciences. Umeå, Sweden.
- Fernandez-Lacruz, R., Edlund, M., Bergström, D., Lindroos, O. 2020. Productivity and profitability of harvesting overgrown roadside verges – a Swedish case study, *International Journal of Forest Engineering*, 32:1, 19-28.
- Forsberg, E. 2010. Buskröjning längs skogsbivägar - En produktivitetsstudie av två kättingslagor. Master's thesis no. 301-2010. Umeå, Sweden, Department of Forest Resource Management, Swedish University of Agricultural Sciences
- Grafström, A. & Lisic, J. 2019. BalancedSampling: Balanced and Spatially Balanced Sampling. R package version 1.5.5. <https://CRAN.R-project.org/package=BalancedSampling>
- Grönlund, Ö. 2021a. Lönsamhet vid avverkning av sly [Profitability of harvesting small trees]. <https://www.skogforsk.se/produkter-och-evenemang/verktyg/lonsamhet-vid-avverkning-av-sly/>
- Iwarsson Wide, M. 2009a. Skogsbränsleuttag i vägkanter - Prestationsstudie. Uttag av skogsbränsle i vägkant med Bracke C16. Uppsala (Sweden): Skogforsk. Report No.: 695–2009.
- Iwarsson Wide, M. 2009b. Skogsbränsleuttag i vägkanter - Prestationsstudie. Uttag av skogsbränsle i vägkant med Ponsse Dual med EH25. Uppsala (Sweden): Skogforsk. report No.: 696–2009.
- Iwarsson Wide, M. 2013. Effektiv volymuppskattning av biomassa i vägkanter och ungskogar med laserdata. Uppsala (Sweden): Skogforsk. Report No.: 804–2013.
- Iwarsson Wide, M., Grönlund, Ö., Von Hofsten, H., Bergström, D., Ekström Larsson, A. 2021. Högeffektiv klenträdsteknik.

- <https://www.skogforsk.se/kunskap/kunskapsbanken/2021/hogeffektiv-kenträdsteknik/>
- Li, H., Jia, Y., Cong, R., Wu ,W., Kwong, STW. & Chen, C. 2021. Superpixel Segmentation Based on Spatially Constrained Subspace Clustering. *IEEE Transactions on Industrial Informatics*, 17, 7501-7512.
- Lindgren, N., Wästlund, A., Bohlin, I., Nyström, K., Nilsson, M., & Olsson, H. 2021. Updating of forest stand data by using recent digital photogrammetry in combination with older airborne laser scanning data. *Scandinavian Journal of Forest Research*, 36(5), 401-407.
- Marklund, L. G. 1988. Biomassafunktioner för tall, gran och björk i Sverige. Umeå, Sweden, Department of Forest Survey, Swedish University of Agricultural Sciences. Rep. 45.
- Mouselimis L. 2022. OpenImageR: An Image Processing Toolkit. R package version 1.2.1, <https://CRAN.R-project.org/package=OpenImageR>
- Nylinder, M., & Kockum, F. 2016. WeCalc – räkna på skogsbränsle. Ed: Wilhelmsson, L. Skogforsk. Uppsala. <https://www.skogforsk.se/produkter-och-evenemang/verktyg/wecalc/>
- Pinheiro, J., Bates, D., R Core Team. 2022. nlme: Linear and Nonlinear Mixed Effects Models. R package version 3.1-157, <https://CRAN.R-project.org/package=nlme>
- Pons, P. & Latapy, M. 2005. Computing Communities in Large Networks Using Random Walks. *Journal of Graph Algorithms and Applications*, 10, 191-218.
- R Core Team. 2021. R: A language and environment for statistical computing. R Foundation for Statistical Computing, Vienna, Austria. URL <https://www.R-project.org/>
- Repolo, J., & Ahnlund Ulvercrona, K. 2014. Modelling biomass of young and dense Scots pine (*Pinus sylvestris* L.) dominated mixed forests in northern Sweden (Vol. 48).
- Roussel, JR. & Auty, D. 2021. Airborne LiDAR Data Manipulation and Visualization for Forestry Applications. R package version 3.2.3. <https://cran.r-project.org/package=lidR>
- Roussel, JR., Auty, D., Coops, NC., Tompalski, P., Goodbody, TRH., Sánchez Meador, A., et al. 2020. lidR: An R package for analysis of Airborne Laser Scanning (ALS) data. *Remote Sensing of Environment*, 251 (August), 112061.
- Skogskunskap. 2016. Vägkantsröjning. <https://www.skogskunskap.se/vagar-i-skogen/drift-och-underhall/sommarunderhall/vagkantsrojning/>
- Skogskunskap. 2021a. Skogsbilvägar och andra enskilda vägar. <https://www.skogskunskap.se/vagar-i-skogen/om-skogsbilvagar/skogsbilvagar-och-andra-enskilda-vagar/>
- Skogskunskap. 2021b. Vägklasser i skogen. <https://www.skogskunskap.se/vagar-i-skogen/om-skogsbilvagar/skogsbilvagar-och-andra-enskilda-vagar/vagklasser-i-skogen/>
- Skogskunskap. 2022. Siffror om vägar. <https://www.skogskunskap.se/vagar-i-skogen/om-skogsbilvagar/skogsbilvagar-och-andra-enskilda-vagar/siffror-om-vagar/>

- Trafikverket. 2019. Drift och underhåll av enskilda vägar. Publikation 2019:186.
- Willén, E. 2021. Geodata åt skogen. Skogforsk kunskapsartikel Nr 77-2021.
<https://www.skogforsk.se/kunskap/kunskapsbanken/2021/geodata-at-skogen-2021/>
- Wood, SN. 2003. Thin plate regression splines. Journal of Royal Statistical Society, 65, 95-114.
- Zellner, A. & Ando, T. 2010. A direct Monte Carlo approach for Bayesian analysis of the seemingly unrelated regression model. Journal of Econometrics 159, 33–45.
- Zellner, A. 1962. An efficient method of estimating seemingly unrelated regression equations and tests for aggregation bias. Journal of the American Statistical Association, 57, 348–368.

Appendix

Appendix 1. Summary of forest inventory data of subplots (transects).

Plot	Subplot	Road class	Coordinates start point ⁽¹⁾			Coordinates end point ⁽¹⁾			Biomass density (dry t ha ⁻¹)		DBH (cm)	Height (m)	Stand density (trees ha ⁻¹)		
			North	East	Height	North	East	Height	Marklund (AGB _M)	Repola & Ulvercrona (AHB _U)					
1	1	9	6659387	638397	39	6659389	638392	39	14.5	8.2	2.3	3.5	2.6	3.5	6,000
1	2	9	6659390	638401	38	6659389	638406	38	11.6	9.4	2.7	4.0	3.6	4.5	6,000
2	3	9	6659353	638357	40	6659357	638354	41	30.9	29.6	3.3	5.2	4.3	6.1	11,000
2	4	9	6659348	638354	40	6659343	638354	41	8.0	7.3	2.2	2.9	3.4	4.1	8,000
3	5	9	6659297	638206	40	6659300	638202	40	1.2	1.1	1.5	1.6	2.9	3.0	3,000
3	6	9	6659294	638207	40	6659289	638209	38	3.0	2.6	1.5	1.6	3.0	3.1	7,000
4	7	9	6657657	639092	40	6657656	639096	40	8.8	7.6	1.9	2.2	3.4	3.4	13,000
4	8	9	6657650	639086	40	6657650	639081	41	30.6	30.9	2.9	4.2	4.3	5.5	17,000
5	9	9	6657566	639091	43	6657567	639096	43	125.9	104.0	6.2	9.8	6.7	9.3	9,000
5	10	9	6657573	639087	43	6657572	639082	42	12.6	12.1	2.2	3.5	3.9	4.8	12,000
6	11	8	6658877	636820	48	6658879	636822	48	5.7	5.0	1.5	1.6	2.9	3.0	14,000
6	12	8	6658870	636821	46	6658866	636819	47	6.4	5.8	1.6	1.7	3.1	3.2	14,000
7	13	8	6658841	636855	48	6658844	636857	47	10.3	10.0	1.8	4.6	3.2	5.9	10,000
7	14	8	6658839	636855	48	6658835	636852	49	7.1	6.1	1.5	1.8	3.2	3.4	16,000
8	15	8	6658720	636936	48	6658721	636941	46	32.8	32.4	2.4	4.7	4.0	6.1	20,000
8	16	8	6658718	636933	48	6658716	636928	49	3.0	2.6	1.2	1.3	2.5	2.6	10,000
9	17	8	6658534	637022	49	6658530	637018	49	41.8	32.9	2.8	5.9	4.0	5.4	14,000
9	18	8	6658524	637031	48	6658527	637035	48	12.1	10.7	1.6	1.9	3.0	3.3	25,000
10	19	8	6658486	637046	47	6658483	637041	47	18.0	17.6	2.1	4.2	3.4	5.4	16,000
10	20	8	6658484	637051	47	6658486	637055	46	25.7	25.5	2.0	4.1	3.6	5.8	23,000

11	21	8	6659753	635007	48	6659749	635009	47	6.6	6.3	1.6	2.4	3.0	3.8	12,000
11	22	8	6659766	635013	48	6659772	635011	50	14.4	14.3	2.4	2.9	3.9	4.4	14,000
12	23	8	6659791	635119	50	6659786	635119	50	2.2	2.1	1.4	1.5	2.8	2.8	6,000
12	24	8	6659801	635123	50	6659806	635123	50	1.9	1.8	1.8	2.3	3.4	4.1	3,000
13	25	9	6669587	634646	41	6669588	634641	42	10.3	9.8	2.3	3.1	3.5	4.1	10,000
13	26	9	6669583	634654	41	6669580	634658	42	6.9	5.1	1.4	1.8	2.7	2.8	13,000
14	27	9	6669538	634635	42	6669540	634630	42	14.5	12.8	3.6	4.7	4.0	4.5	5,000
14	28	9	6669538	634643	42	6669537	634648	42	6.1	5.2	2.4	3.0	3.3	3.8	5,000
15	29	9	6668816	633286	46	6668819	633283	46	7.0	6.8	2.1	2.4	3.7	4.0	9,000
15	30	9	6668810	633288	46	6668806	633291	47	45.4	30.2	2.6	4.9	3.1	4.4	16,000
16	31	9	6668795	633256	46	6668798	633253	48	10.5	10.3	2.3	4.0	3.9	5.3	8,000
16	32	9	6668789	633259	46	6668787	633262	46	23.0	17.1	3.4	6.1	4.1	5.8	5,000
17	33	9	6669401	632535	49	6669401	632531	46	0.7	0.7	1.5	1.5	2.7	2.7	2,000
17	34	9	6669386	632531	44	6669382	632533	44	8.4	6.4	1.6	3.0	2.9	3.4	10,000
18	35	9	6667066	640631	57	6667069	640637	57	4.9	4.5	1.6	2.1	3.0	3.6	10,000
18	36	9	6667060	640632	56	6667057	640628	60	(no trees)	-	-	-	-	-	-
19	37	9	6667014	640684	55	6667016	640689	56	9.7	10.1	3.8	4.8	5.4	6.5	3,000
19	38	9	6667001	640687	55	6666998	640682	56	4.3	2.3	1.5	1.8	2.3	2.1	4,000
20	39	9	6667217	641099	55	6667215	641096	55	1.9	1.8	1.8	2.5	3.4	4.1	3,000
20	40	9	6667223	641102	55	6667225	641106	56	88.7	72.3	3.8	8.7	4.8	7.3	18,000
21	41	9	6665980	641841	49	6665980	641846	49	8.8	8.2	1.7	2.4	3.3	3.6	15,000
21	42	9	6665972	641839	49	6665970	641836	49	10.0	5.2	2.0	2.6	2.2	2.6	5,000
22	43	9	6666057	641765	48	6666063	641764	49	6.9	6.7	2.0	3.2	3.2	4.1	8,000
22	44	9	6666046	641752	47	6666041	641753	47	19.8	18.4	2.2	4.0	3.4	4.8	16,000
23	45	9	6666034	641596	46	6666039	641595	48	31.5	31.6	2.7	4.4	4.2	6.1	18,000
23	46	9	6666020	641607	46	6666016	641608	46	1.8	2.2	2.7	2.7	2.9	2.9	2,000
24	47	8	6666321	640555	48	6666325	640551	47	44.0	39.0	3.0	6.4	4.3	6.3	13,000
24	48	8	6666307	640553	46	6666303	640556	47	11.4	11.2	2.8	4.7	2.8	3.6	7,000
25	49	9	6654948	645055	35	6654945	645051	35	8.8	7.9	2.2	3.1	3.4	4.3	8,000
25	50	9	6654958	645055	35	6654961	645058	37	2.3	2.1	1.3	1.4	2.7	2.8	7,000

26	51	9	6655009	645010	36	6655007	645005	37	10.0	10.3	3.9	4.8	3.7	4.2	4,000
26	52	9	6655010	645015	36	6655011	645020	35	0.9	1.0	2.6	2.6	3.3	3.3	1,000
27	53	9	6652869	645787	39	6652863	645788	39	36.8	34.6	1.8	2.9	3.3	4.3	52,000
27	54	9	6652874	645785	39	6652879	645784	41	56.8	50.3	2.6	7.9	3.6	5.8	21,000
28	55	8	6653736	646254	32	6653733	646251	33	60.1	49.7	3.9	9.3	4.2	6.2	8,000
28	56	8	6653732	646273	32	6653735	646277	32	25.6	23.7	3.4	4.3	4.6	5.0	10,000
29	57	8	6653792	646189	36	6653791	646185	37	16.6	12.4	3.5	4.2	4.1	4.6	5,000
29	58	8	6653806	646192	34	6653808	646195	39	82.4	74.8	5.3	7.4	6.1	7.8	10,000
30	59	8	6653149	636717	45	6653145	636714	44	3.6	3.3	1.6	1.8	2.9	3.1	8,000
30	60	8	6653141	636732	45	6653145	636735	46	10.7	8.3	3.4	6.6	3.1	3.7	3,000
31	61	8	6653064	636812	48	6653060	636809	47	15.0	9.6	2.9	3.2	2.7	3.0	6,000
31	62	8	6653062	636821	47	6653066	636824	47	10.9	9.3	2.0	2.7	3.2	3.4	13,000
32	63	9	6654586	635849	51	6654584	635853	56	13.4	13.8	3.1	5.1	5.0	7.6	5,000
32	64	9	6654595	635850	52	6654599	635848	53	21.6	21.6	3.1	5.0	4.8	6.5	9,000
33	65	9	6654617	635934	52	6654611	635935	52	3.4	2.4	1.4	1.5	2.7	2.8	6,000
33	66	9	6654621	635927	52	6654626	635926	52	7.5	7.5	2.5	3.3	4.2	5.1	6,000
34	67	9	6654913	636391	50	6654910	636387	50	49.4	48.4	2.3	4.3	3.8	5.6	35,000
34	68	9	6654923	636391	49	6654925	636395	50	69.2	48.6	3.7	8.5	4.0	6.4	13,000
35	69	8	6651394	628744	73	6651395	628740	75	1.9	2.0	2.3	3.2	3.4	4.0	2,000
35	70	8	6651395	628753	73	6651394	628759	72	59.0	53.6	3.9	7.6	4.9	8.0	11,000
36	71	8	6651472	628768	73	6651473	628773	72	38.0	33.2	3.0	4.7	3.7	4.8	16,000
36	72	8	6651469	628760	73	6651470	628755	73	17.7	18.4	3.1	4.5	4.0	5.3	9,000
37	73	8	6651577	628791	71	6651576	628797	71	61.7	52.6	3.1	9.8	4.0	8.5	15,000
37	74	8	6651572	628782	72	6651574	628777	72	0.7	0.6	2.0	2.0	3.8	3.8	1,000
38	75	9	6651268	627827	67	6651271	627830	67	54.5	43.6	3.0	5.2	3.9	5.4	18,000
38	76	9	6651263	627821	66	6651261	627816	69	1.7	1.6	1.5	1.9	2.9	3.5	4,000
39	77	8	6660215	646084	30	6660220	646082	31	39.4	37.4	4.1	6.2	4.5	6.0	10,000
39	78	8	6660191	646079	30	6660190	646083	30	5.1	5.4	2.0	3.6	3.2	5.3	5,000
40	79	8	6660141	646058	30	6660143	646054	29	132.9	121.5	5.7	8.2	7.0	9.2	13,000
40	80	8	6660144	646068	30	6660144	646073	30	2.1	2.0	1.4	1.5	2.6	2.8	6,000

41	81	9	6660127	646865	28	6660129	646860	28	35.0	34.9	2.4	3.6	4.2	5.5	27,000
41	82	9	6660120	646871	28	6660118	646875	31	40.2	40.9	2.8	3.9	4.8	5.8	23,000
42	83	9	6660244	646831	29	6660242	646825	29	26.3	23.5	3.3	4.3	4.6	5.7	10,000
42	84	9	6660250	646836	25	6660251	646841	28	1.8	0.9	1.9	1.9	4.5	4.5	1,000
43	85	9	6660061	645758	30	6660063	645761	31	11.4	8.1	2.8	3.6	3.1	3.6	5,000
43	86	9	6660056	645755	30	6660054	645751	30	14.1	9.4	2.6	3.1	3.5	3.9	7,000
44	87	9	6660115	645720	31	6660117	645724	31	22.5	19.4	2.9	7.6	4.0	7.6	6,000
44	88	9	6660110	645714	31	6660108	645711	32	41.2	37.7	5.3	7.2	5.7	6.8	6,000
45	89	9	6660159	645696	31	6660156	645689	30	19.9	19.3	4.7	6.1	5.6	6.5	4,000
45	90	9	6660152	645686	31	6660163	645699	31	9.7	5.3	1.5	1.9	2.4	2.5	9,000
46	91	9	6660174	645628	31	6660179	645627	31	9.6	5.9	2.1	2.8	2.9	3.1	6,000
46	92	9	6660169	645630	31	6660164	645631	31	19.5	14.0	2.4	3.3	3.3	3.5	12,000
47	93	9	6666773	647102	34	6666778	647102	34	4.0	3.6	1.4	1.5	2.7	2.8	11,000
47	94	9	6666770	647104	34	6666765	647104	34	12.6	11.9	1.7	2.2	3.1	3.6	23,000
48	95	9	6666777	646962	35	6666782	646961	35	27.2	22.1	2.1	5.3	3.1	3.9	23,000
48	96	9	6666773	646953	35	6666768	646954	35	47.0	39.4	3.1	6.9	3.3	4.1	13,000
49	97	9	6666822	646893	36	6666819	646897	37	23.8	23.6	2.8	4.4	4.1	5.4	14,000
49	98	9	6666827	646890	36	6666830	646887	35	5.0	4.7	1.9	2.2	3.4	3.6	8,000
50	99	9	6666932	646912	36	6666932	646917	36	6.3	6.4	3.1	3.6	4.3	4.5	4,000
50	100	9	6666933	646907	36	6666933	646902	36	23.1	15.3	4.2	5.2	3.4	3.9	4,000

(1) According to SWEREF 99 TM coordinate system. Height above sea level (m).

Appendix 2. STAN model formulation.

// generated with brms 2.16.3

```
/* VARIABLES:  
 * Responses:  
 * Heightar - arithmetic tree height  
 * DBHar - arithmetic DBH  
 * drythaM - aboveground biomass estimates from Marklund models (Mg/ha)  
 * drythaU - aboveground biomass estimates from Repola & Ulvcrona models (Mg/ha)  
  
 * Covariates with hyperbolic arcsine transformation (asinh):  
 * zmu - mean echo height  
 * zP95 - 95th percentile of the echo height distribution  
 * zP75 - 75th percentile of the echo height distribution  
 * zsd - the standard deviation of the echo height distribution  
 * zD30 - the proportions of echo heights above 3m  
  
 */  
  
/*/  
functions {  
    /* compute correlated group-level effects  
     * Args:  
     * z: matrix of unscaled group-level effects  
     * SD: vector of standard deviation parameters  
     * L: Cholesky factor correlation matrix  
     * Returns:  
     * matrix of scaled group-level effects  
    */  
    matrix scale_r_cor(matrix z, vector SD, matrix L) {  
        // r is stored in another dimension order than z  
        return transpose(diag_pre_multiply(SD, L) * z);  
    }  
}  
data {  
    int<lower=1> N; // total number of observations  
    int<lower=1> N_Heightar; // number of observations  
    vector[N_Heightar] Y_Heightar; // response variable  
    // data for splines  
    int Ks_Heightar; // number of linear effects  
    matrix[N_Heightar, Ks_Heightar] Xs_Heightar; // design matrix for the linear effects  
    // data for spline s(asinh(zmu), k = k.s, bs = bs.model)
```

```

int nb_Heightar_1; // number of bases
int knots_Heightar_1[nb_Heightar_1]; // number of knots
// basis function matrices
matrix[N_Heightar, knots_Heightar_1[1]] Zs_Heightar_1_1;
// data for spline s(asinh(zP95), k = k.s, bs = bs.model)
int nb_Heightar_2; // number of bases
int knots_Heightar_2[nb_Heightar_2]; // number of knots
// basis function matrices
matrix[N_Heightar, knots_Heightar_2[1]] Zs_Heightar_2_1;
// data for spline s(asinh(zsd), k = k.s, bs = bs.model)
int nb_Heightar_3; // number of bases
int knots_Heightar_3[nb_Heightar_3]; // number of knots
// basis function matrices
matrix[N_Heightar, knots_Heightar_3[1]] Zs_Heightar_3_1;
int<lower=1> N_DBHar; // number of observations
vector[N_DBHar] Y_DBHar; // response variable
// data for splines
int Ks_DBHar; // number of linear effects
matrix[N_DBHar, Ks_DBHar] Xs_DBHar; // design matrix for the linear effects
// data for spline s(asinh(zD30), k = k.s, bs = bs.model)
int nb_DBHar_1; // number of bases
int knots_DBHar_1[nb_DBHar_1]; // number of knots
// basis function matrices
matrix[N_DBHar, knots_DBHar_1[1]] Zs_DBHar_1_1;
// data for spline s(asinh(zP75), k = k.s, bs = bs.model)
int nb_DBHar_2; // number of bases
int knots_DBHar_2[nb_DBHar_2]; // number of knots
// basis function matrices
matrix[N_DBHar, knots_DBHar_2[1]] Zs_DBHar_2_1;
// data for spline s(asinh(zsd), k = k.s, bs = bs.model)
int nb_DBHar_3; // number of bases
int knots_DBHar_3[nb_DBHar_3]; // number of knots
// basis function matrices
matrix[N_DBHar, knots_DBHar_3[1]] Zs_DBHar_3_1;
// data for spline s(asinh(zmu), k = k.s, bs = bs.model)
int nb_DBHar_4; // number of bases
int knots_DBHar_4[nb_DBHar_4]; // number of knots
// basis function matrices
matrix[N_DBHar, knots_DBHar_4[1]] Zs_DBHar_4_1;
int<lower=1> N_drythaM; // number of observations
vector[N_drythaM] Y_drythaM; // response variable
// data for splines
int Ks_drythaM; // number of linear effects
matrix[N_drythaM, Ks_drythaM] Xs_drythaM; // design matrix for the linear effects

```

```

// data for spline s(asinh(zP95), k = k.s, bs = bs.model)
int nb_drythaM_1; // number of bases
int knots_drythaM_1[nb_drythaM_1]; // number of knots
// basis function matrices
matrix[N_drythaM, knots_drythaM_1[1]] Zs_drythaM_1_1;
// data for spline s(asinh(zP75), k = k.s, bs = bs.model)
int nb_drythaM_2; // number of bases
int knots_drythaM_2[nb_drythaM_2]; // number of knots
// basis function matrices
matrix[N_drythaM, knots_drythaM_2[1]] Zs_drythaM_2_1;
// data for spline s(asinh(zsd), k = k.s, bs = bs.model)
int nb_drythaM_3; // number of bases
int knots_drythaM_3[nb_drythaM_3]; // number of knots
// basis function matrices
matrix[N_drythaM, knots_drythaM_3[1]] Zs_drythaM_3_1;
int<lower=1> N_drythaU; // number of observations
vector[N_drythaU] Y_drythaU; // response variable
// data for splines
int Ks_drythaU; // number of linear effects
matrix[N_drythaU, Ks_drythaU] Xs_drythaU; // design matrix for the linear effects
// data for spline s(asinh(zP95), k = k.s, bs = bs.model)
int nb_drythaU_1; // number of bases
int knots_drythaU_1[nb_drythaU_1]; // number of knots
// basis function matrices
matrix[N_drythaU, knots_drythaU_1[1]] Zs_drythaU_1_1;
// data for spline s(asinh(zP75), k = k.s, bs = bs.model)
int nb_drythaU_2; // number of bases
int knots_drythaU_2[nb_drythaU_2]; // number of knots
// basis function matrices
matrix[N_drythaU, knots_drythaU_2[1]] Zs_drythaU_2_1;
// data for spline s(asinh(zsd), k = k.s, bs = bs.model)
int nb_drythaU_3; // number of bases
int knots_drythaU_3[nb_drythaU_3]; // number of knots
// basis function matrices
matrix[N_drythaU, knots_drythaU_3[1]] Zs_drythaU_3_1;
int<lower=1> nresp; // number of responses
int nrescor; // number of residual correlations
// data for group-level effects of ID 1
int<lower=1> N_1; // number of grouping levels
int<lower=1> M_1; // number of coefficients per level
int<lower=1> J_1_Heightar[N_Heightar]; // grouping indicator per observation
int<lower=1> J_1_DBHar[N_DBHar]; // grouping indicator per observation
int<lower=1> J_1_drythaM[N_drythaM]; // grouping indicator per observation
int<lower=1> J_1_drythaU[N_drythaU]; // grouping indicator per observation

```

```

// group-level predictor values
vector[N_Heightar] Z_1_Heightar_1;
vector[N_DBHar] Z_1_DBHar_2;
vector[N_drythaM] Z_1_drythaM_3;
vector[N_drythaU] Z_1_drythaU_4;
int<lower=1> NC_1; // number of group-level correlations
int prior_only; // should the likelihood be ignored?
}

transformed data {
vector[nresp] Y[N]; // response array
for (n in 1:N) {
Y[n] = transpose([Y_Heightar[n], Y_DBHar[n], Y_drythaM[n], Y_drythaU[n]]);
}
}

parameters {
real Intercept_Heightar; // temporary intercept for centered predictors
vector[Ks_Heightar] bs_Heightar; // spline coefficients
// parameters for spline s(asinh(zmu), k = k.s, bs = bs.model)
// standarized spline coefficients
vector[knots_Heightar_1[1]] zs_Heightar_1_1;
real<lower=0> sds_Heightar_1_1; // standard deviations of spline coefficients
// parameters for spline s(asinh(zP95), k = k.s, bs = bs.model)
// standarized spline coefficients
vector[knots_Heightar_2[1]] zs_Heightar_2_1;
real<lower=0> sds_Heightar_2_1; // standard deviations of spline coefficients
// parameters for spline s(asinh(zsd), k = k.s, bs = bs.model)
// standarized spline coefficients
vector[knots_Heightar_3[1]] zs_Heightar_3_1;
real<lower=0> sds_Heightar_3_1; // standard deviations of spline coefficients
real<lower=0> sigma_Heightar; // dispersion parameter
real Intercept_DBHar; // temporary intercept for centered predictors
vector[Ks_DBHar] bs_DBHar; // spline coefficients
// parameters for spline s(asinh(zD30), k = k.s, bs = bs.model)
// standarized spline coefficients
vector[knots_DBHar_1[1]] zs_DBHar_1_1;
real<lower=0> sds_DBHar_1_1; // standard deviations of spline coefficients
// parameters for spline s(asinh(zP75), k = k.s, bs = bs.model)
// standarized spline coefficients
vector[knots_DBHar_2[1]] zs_DBHar_2_1;
real<lower=0> sds_DBHar_2_1; // standard deviations of spline coefficients
// parameters for spline s(asinh(zsd), k = k.s, bs = bs.model)
// standarized spline coefficients
vector[knots_DBHar_3[1]] zs_DBHar_3_1;
real<lower=0> sds_DBHar_3_1; // standard deviations of spline coefficients

```

```

// parameters for spline s(asinh(zmu), k = k.s, bs = bs.model)
// standarized spline coefficients
vector[knots_DBHar_4[1]] zs_DBHar_4_1;
real<lower=0> sds_DBHar_4_1; // standard deviations of spline coefficients
real<lower=0> sigma_DBHar; // dispersion parameter
real Intercept_drythaM; // temporary intercept for centered predictors
vector[Ks_drythaM] bs_drythaM; // spline coefficients
// parameters for spline s(asinh(zP95), k = k.s, bs = bs.model)
// standarized spline coefficients
vector[knots_drythaM_1[1]] zs_drythaM_1_1;
real<lower=0> sds_drythaM_1_1; // standard deviations of spline coefficients
// parameters for spline s(asinh(zP75), k = k.s, bs = bs.model)
// standarized spline coefficients
vector[knots_drythaM_2[1]] zs_drythaM_2_1;
real<lower=0> sds_drythaM_2_1; // standard deviations of spline coefficients
// parameters for spline s(asinh(zsd), k = k.s, bs = bs.model)
// standarized spline coefficients
vector[knots_drythaM_3[1]] zs_drythaM_3_1;
real<lower=0> sds_drythaM_3_1; // standard deviations of spline coefficients
real<lower=0> sigma_drythaM; // dispersion parameter
real Intercept_drythaU; // temporary intercept for centered predictors
vector[Ks_drythaU] bs_drythaU; // spline coefficients
// parameters for spline s(asinh(zP95), k = k.s, bs = bs.model)
// standarized spline coefficients
vector[knots_drythaU_1[1]] zs_drythaU_1_1;
real<lower=0> sds_drythaU_1_1; // standard deviations of spline coefficients
// parameters for spline s(asinh(zP75), k = k.s, bs = bs.model)
// standarized spline coefficients
vector[knots_drythaU_2[1]] zs_drythaU_2_1;
real<lower=0> sds_drythaU_2_1; // standard deviations of spline coefficients
// parameters for spline s(asinh(zsd), k = k.s, bs = bs.model)
// standarized spline coefficients
vector[knots_drythaU_3[1]] zs_drythaU_3_1;
real<lower=0> sds_drythaU_3_1; // standard deviations of spline coefficients
real<lower=0> sigma_drythaU; // dispersion parameter
cholesky_factor_corr[nresp] Lrescor; // parameters for multivariate linear models
vector<lower=0>[M_1] sd_1; // group-level standard deviations
matrix[M_1, N_1] z_1; // standarized group-level effects
cholesky_factor_corr[M_1] L_1; // Cholesky factor of correlation matrix
}

transformed parameters {
    // actual spline coefficients
    vector[knots_Heightar_1[1]] s_Heightar_1_1;
    // actual spline coefficients
}

```

```

vector[knots_Heightar_2[1]] s_Heightar_2_1;
// actual spline coefficients
vector[knots_Heightar_3[1]] s_Heightar_3_1;
// actual spline coefficients
vector[knots_DBHar_1[1]] s_DBHar_1_1;
// actual spline coefficients
vector[knots_DBHar_2[1]] s_DBHar_2_1;
// actual spline coefficients
vector[knots_DBHar_3[1]] s_DBHar_3_1;
// actual spline coefficients
vector[knots_DBHar_4[1]] s_DBHar_4_1;
// actual spline coefficients
vector[knots_drythaM_1[1]] s_drythaM_1_1;
// actual spline coefficients
vector[knots_drythaM_2[1]] s_drythaM_2_1;
// actual spline coefficients
vector[knots_drythaM_3[1]] s_drythaM_3_1;
// actual spline coefficients
vector[knots_drythaU_1[1]] s_drythaU_1_1;
// actual spline coefficients
vector[knots_drythaU_2[1]] s_drythaU_2_1;
// actual spline coefficients
vector[knots_drythaU_3[1]] s_drythaU_3_1;
matrix[N_1, M_1] r_1; // actual group-level effects
// using vectors speeds up indexing in loops
vector[N_1] r_1_Heightar_1;
vector[N_1] r_1_DBHar_2;
vector[N_1] r_1_drythaM_3;
vector[N_1] r_1_drythaU_4;
// compute actual spline coefficients
s_Heightar_1_1 = sds_Heightar_1_1 * zs_Heightar_1_1;
// compute actual spline coefficients
s_Heightar_2_1 = sds_Heightar_2_1 * zs_Heightar_2_1;
// compute actual spline coefficients
s_Heightar_3_1 = sds_Heightar_3_1 * zs_Heightar_3_1;
// compute actual spline coefficients
s_DBHar_1_1 = sds_DBHar_1_1 * zs_DBHar_1_1;
// compute actual spline coefficients
s_DBHar_2_1 = sds_DBHar_2_1 * zs_DBHar_2_1;
// compute actual spline coefficients
s_DBHar_3_1 = sds_DBHar_3_1 * zs_DBHar_3_1;
// compute actual spline coefficients
s_DBHar_4_1 = sds_DBHar_4_1 * zs_DBHar_4_1;
// compute actual spline coefficients

```

```

s_drythaM_1_1 = sds_drythaM_1_1 * zs_drythaM_1_1;
// compute actual spline coefficients
s_drythaM_2_1 = sds_drythaM_2_1 * zs_drythaM_2_1;
// compute actual spline coefficients
s_drythaM_3_1 = sds_drythaM_3_1 * zs_drythaM_3_1;
// compute actual spline coefficients
s_drythaU_1_1 = sds_drythaU_1_1 * zs_drythaU_1_1;
// compute actual spline coefficients
s_drythaU_2_1 = sds_drythaU_2_1 * zs_drythaU_2_1;
// compute actual spline coefficients
s_drythaU_3_1 = sds_drythaU_3_1 * zs_drythaU_3_1;
// compute actual group-level effects
r_1 = scale_r_cor(z_1, sd_1, L_1);
r_1_Heighttar_1 = r_1[, 1];
r_1_DBHar_2 = r_1[, 2];
r_1_drythaM_3 = r_1[, 3];
r_1_drythaU_4 = r_1[, 4];
}
model {
// likelihood including constants
if (!prior_only) {
// initialize linear predictor term
vector[N_Heighttar] mu_Heighttar = Intercept_Heighttar + rep_vector(o.o, N_Heighttar) + Xs_Heighttar *
bs_Heighttar + Zs_Heighttar_1_1 * s_Heighttar_1_1 + Zs_Heighttar_2_1 * s_Heighttar_2_1 + Zs_Heighttar_3_1 *
s_Heighttar_3_1;
// initialize linear predictor term
vector[N_DBHar] mu_DBHar = Intercept_DBHar + rep_vector(o.o, N_DBHar) + Xs_DBHar * bs_DBHar +
Zs_DBHar_1_1 * s_DBHar_1_1 + Zs_DBHar_2_1 * s_DBHar_2_1 + Zs_DBHar_3_1 * s_DBHar_3_1 +
Zs_DBHar_4_1 * s_DBHar_4_1;
// initialize linear predictor term
vector[N_drythaM] mu_drythaM = Intercept_drythaM + rep_vector(o.o, N_drythaM) + Xs_drythaM *
bs_drythaM + Zs_drythaM_1_1 * s_drythaM_1_1 + Zs_drythaM_2_1 * s_drythaM_2_1 + Zs_drythaM_3_1 *
s_drythaM_3_1;
// initialize linear predictor term
vector[N_drythaU] mu_drythaU = Intercept_drythaU + rep_vector(o.o, N_drythaU) + Xs_drythaU *
bs_drythaU + Zs_drythaU_1_1 * s_drythaU_1_1 + Zs_drythaU_2_1 * s_drythaU_2_1 + Zs_drythaU_3_1 *
s_drythaU_3_1;
// multivariate predictor array
vector[nresp] Mu[N];
vector[nresp] sigma = transpose([sigma_Heighttar, sigma_DBHar, sigma_drythaM, sigma_drythaU]);
// Cholesky factor of residual covariance matrix
matrix[nresp, nresp] LSigma = diag_pre_multiply(sigma, Lrescor);
for (n in 1:N_Heighttar) {
// add more terms to the linear predictor
mu_Heighttar[n] += r_1_Heighttar_1[J_1_Heighttar[n]] * Z_1_Heighttar_1[n];
}
for (n in 1:N_DBHar) {
}
}

```

```

// add more terms to the linear predictor
mu_DBHar[n] += r_1_DBHar_2[J_1_DBHar[n]] * Z_1_DBHar_2[n];
}

for (n in 1:N_drythaM) {
    // add more terms to the linear predictor
    mu_drythaM[n] += r_1_drythaM_3[J_1_drythaM[n]] * Z_1_drythaM_3[n];
}

for (n in 1:N_drythaU) {
    // add more terms to the linear predictor
    mu_drythaU[n] += r_1_drythaU_4[J_1_drythaU[n]] * Z_1_drythaU_4[n];
}

for (n in 1:N_Heightar) {
    // apply the inverse link function
    mu_Heightar[n] = exp(mu_Heightar[n]);
}

for (n in 1:N_DBHar) {
    // apply the inverse link function
    mu_DBHar[n] = exp(mu_DBHar[n]);
}

for (n in 1:N_drythaM) {
    // apply the inverse link function
    mu_drythaM[n] = exp(mu_drythaM[n]);
}

for (n in 1:N_drythaU) {
    // apply the inverse link function
    mu_drythaU[n] = exp(mu_drythaU[n]);
}

// combine univariate parameters
for (n in 1:N) {
    Mu[n] = transpose([mu_Heightar[n], mu_DBHar[n], mu_drythaM[n], mu_drythaU[n]]);
}

target += multi_normal_cholesky_lpdf(Y | Mu, LSigma);
}

// priors including constants
target += student_t_lpdf(Intercept_Heightar | 3, 1.2, 2.5);
target += student_t_lpdf(sds_Heightar_1_1 | 3, 0, 2.5)
- 1 * student_t_lccdf(0 | 3, 0, 2.5);
target += std_normal_lpdf(zs_Heightar_1_1);
target += student_t_lpdf(sds_Heightar_2_1 | 3, 0, 2.5)
- 1 * student_t_lccdf(0 | 3, 0, 2.5);
target += std_normal_lpdf(zs_Heightar_2_1);
target += student_t_lpdf(sds_Heightar_3_1 | 3, 0, 2.5)
- 1 * student_t_lccdf(0 | 3, 0, 2.5);
target += std_normal_lpdf(zs_Heightar_3_1);

```

```

target += student_t_lpdf(sigma_Heightar | 3, 0, 2.5)
- 1 * student_t_lccdf(o | 3, 0, 2.5);
target += student_t_lpdf(Intercept_DBHar | 3, 0.9, 2.5);
target += student_t_lpdf(sds_DBHar_1_1 | 3, 0, 2.5)
- 1 * student_t_lccdf(o | 3, 0, 2.5);
target += std_normal_lpdf(zs_DBHar_1_1);
target += student_t_lpdf(sds_DBHar_2_1 | 3, 0, 2.5)
- 1 * student_t_lccdf(o | 3, 0, 2.5);
target += std_normal_lpdf(zs_DBHar_2_1);
target += student_t_lpdf(sds_DBHar_3_1 | 3, 0, 2.5)
- 1 * student_t_lccdf(o | 3, 0, 2.5);
target += std_normal_lpdf(zs_DBHar_3_1);
target += student_t_lpdf(sds_DBHar_4_1 | 3, 0, 2.5)
- 1 * student_t_lccdf(o | 3, 0, 2.5);
target += std_normal_lpdf(zs_DBHar_4_1);
target += student_t_lpdf(sigma_DBHar | 3, 0, 2.5)
- 1 * student_t_lccdf(o | 3, 0, 2.5);
target += student_t_lpdf(Intercept_drythaM | 3, 2.4, 2.5);
target += student_t_lpdf(sds_drythaM_1_1 | 3, 0, 2.5)
- 1 * student_t_lccdf(o | 3, 0, 2.5);
target += std_normal_lpdf(zs_drythaM_1_1);
target += student_t_lpdf(sds_drythaM_2_1 | 3, 0, 2.5)
- 1 * student_t_lccdf(o | 3, 0, 2.5);
target += std_normal_lpdf(zs_drythaM_2_1);
target += student_t_lpdf(sds_drythaM_3_1 | 3, 0, 2.5)
- 1 * student_t_lccdf(o | 3, 0, 2.5);
target += std_normal_lpdf(zs_drythaM_3_1);
target += student_t_lpdf(sigma_drythaM | 3, 0, 12.5)
- 1 * student_t_lccdf(o | 3, 0, 12.5);
target += student_t_lpdf(Intercept_drythaU | 3, 2.3, 2.5);
target += student_t_lpdf(sds_drythaU_1_1 | 3, 0, 2.5)
- 1 * student_t_lccdf(o | 3, 0, 2.5);
target += std_normal_lpdf(zs_drythaU_1_1);
target += student_t_lpdf(sds_drythaU_2_1 | 3, 0, 2.5)
- 1 * student_t_lccdf(o | 3, 0, 2.5);
target += std_normal_lpdf(zs_drythaU_2_1);
target += student_t_lpdf(sds_drythaU_3_1 | 3, 0, 2.5)
- 1 * student_t_lccdf(o | 3, 0, 2.5);
target += std_normal_lpdf(zs_drythaU_3_1);
target += student_t_lpdf(sigma_drythaU | 3, 0, 11.5)
- 1 * student_t_lccdf(o | 3, 0, 11.5);
target += lkj_corr_cholesky_lpdf(Lrescor | 1);
target += student_t_lpdf(sd_1 | 3, 0, 2.5)
- 4 * student_t_lccdf(o | 3, 0, 2.5);

```

```

target += std_normal_lpdf(to_vector(z_1));
target += lkj_corr_cholesky_lpdf(L_1 | 1);
}

generated quantities {
    // actual population-level intercept
    real b_Heightar_Intercept = Intercept_Heightar;
    // actual population-level intercept
    real b_DBHar_Intercept = Intercept_DBHar;
    // actual population-level intercept
    real b_drythaM_Intercept = Intercept_drythaM;
    // actual population-level intercept
    real b_drythaU_Intercept = Intercept_drythaU;
    // residual correlations
    corr_matrix[nresp] Rescor = multiply_lower_tri_self_transpose(Lrescor);
    vector<lower=-1,upper=1>[nrescor] rescor;
    // compute group-level correlations
    corr_matrix[M_1] Cor_1 = multiply_lower_tri_self_transpose(L_1);
    vector<lower=-1,upper=1>[NC_1] cor_1;
    // extract upper diagonal of correlation matrix
    for (k in 1:nresp) {
        for (j in 1:(k - 1)) {
            rescor[choose(k - 1, 2) + j] = Rescor[j, k];
        }
    }
    // extract upper diagonal of correlation matrix
    for (k in 1:M_1) {
        for (j in 1:(k - 1)) {
            cor_1[choose(k - 1, 2) + j] = Cor_1[j, k];
        }
    }
}

```